A Hierarchy of Biomolecular Proportional-Integral-Derivative Feedback Controllers for Robust Perfect Adaptation and Dynamic Performance

Maurice Filo[1] and Mustafa Khammash[1,*]

[1]ETH Zürich Department of Biosystems Science and Engineering
[*]Correspondence: mustafa.khammash@bsse.ethz.ch

Abstract

Proportional-Integral-Derivative (PID) feedback controllers have been the most widely used controllers in industry for almost a century due to their good performance, simplicity, and ease of tuning. Motivated by their success in various engineering disciplines, PID controllers recently found their way into synthetic biology, where the design of feedback molecular control systems has been identified as an important goal. In this paper, we consider the mathematical realization of PID controllers via biomolecular interactions. We propose an array of topologies that offer a compromise between simplicity and high performance. We first demonstrate that different Proportional-Integral (PI) controllers exhibit different capabilities for enhancing the dynamics and reducing variance (cell-to-cell variability). Next, we introduce several derivative controllers that are realized based on incoherent feedforward loops acting in a feedback configuration. Alternatively, we show that differentiators can be realized by placing molecular integrators in a negative feedback loop—an arrangement that can then be augmented by PI components to yield PID feedback controllers. We demonstrate that the derivative component can be exploited for enhancing system stability, dramatically increasing the molecular control system's dynamic performance, and for reducing the noise effect on the output of interest. The PID controller features are established through various deterministic and stochastic analyses as well as numerical simulations. The large array of novel biomolecular PID controllers introduced here constitutes a conceptual and practical advancement in cybergenetics, and present a basis for the design and construction of advanced high-performance biomolecular control systems that robustly regulate the dynamics of living systems.

One of the most salient features of biological systems is their ability to adapt to their noisy environments. For example, cells often regulate gene expression to counteract all sorts of intrinsic and extrinsic noise in order to maintain a desirable behavior in a precise and timely fashion. This resilience toward undesired disturbances is often achieved via feedback control that has proved to be ubiquitous in both natural (e.g. [2–4]) and engineered systems (e.g. [5,6]). In fact, synthetically engineering biomolecular controllers is gaining a wide attention from biologists and engineers (e.g. [7–15]).

A standard general setup for feedback controllers is depicted as a block diagram (refer to Box 1. A Primer on Block Diagrams in the SI) in Figure 1(a). The "Plant" block represents the process to be controlled. It can be actuated through its input, denoted here by u, to dynamically manipulate its output of interest, denoted here by y. The objective of such control systems is to design a feedback controller that *automatically* actuates the plant in a smart autonomous fashion and guarantees that the output y meets certain performance goals despite the presence of disturbances in the plant. These performance goals, described in Figure 1(b), include (but are not limited to) Robust Perfect Adaptation (RPA), stability enhancement, desirable transient response and variance reduction. Control theory developed a wide set of tools to design feedback controllers that meet certain performance objectives. For instance, it is well known in control theory (internal model principle [16]) that a controller should involve an Integral (I) action to be able to achieve RPA. Furthermore, Proportional-Integral-Derivative (PID) feedback controllers – first rigorously introduced by Nicolas Minorsky [17] around a hundred years ago – adds a Proportional (P) and Derivative (D) action to the Integrator (I) to be able to tune the transient dynamics and enhance stability while preserving RPA. Interestingly, after almost a century, PID controllers are still the most widely used controllers in industrial applications spanning a broad range of engineering disciplines such as mechanical and electrical engineering [18–20].

Originally, PID feedback controllers were designed to control mechanical (later, electrical) systems such as automatic ship steering (later, telephone engineering systems) [21]. Such control systems involve controlling quantities that can take both negative and positive values such as angles, velocities, electric currents, voltages, etc... Furthermore, traditional PID controllers possess linear dynamics since all three operations of a PID are linear. Two classes of linear PID controllers, adopted from [22, Chapter 10], are shown in Figures 1(c) and (d). In Figure 1(c), the error signal $e(t) := r - y(t)$ is fed into the three (P, I, and D) components. The outputs of the three components are summed up to yield the control action u which serves as the actuation input to the plant. However, in Figure 1(d), the controller has two degrees of freedom since both the error e and the output y are used separately and simultaneously. Particularly, the error is fed into the integrator, while the output is fed into the proportional and derivative components. Observe that both architectures require that the integrator operates on the error (and not the output). This is necessary to achieve RPA and can be easily seen using a very simple argument explained next. Let $u_I(t)$ denote the output of the integrator, that is

$$u_I(t) := K_I \int_0^t e(\tau)d\tau \quad \Longrightarrow \quad \dot{u}_I(t) = K_I e(t). \tag{1}$$

Assuming that the dynamics are stable, then at steady state we have $\lim_{t\to\infty} \dot{u}_I(t) = 0$. This implies that, at steady state, the error $e := r - y$ has to be zero, and thus $\lim_{t\to\infty} y(t) = r$, hence achieving the steady-state tracking property. Observe that this argument does not depend on the plant, hence achieving the robustness property.

For mechanical and electrical systems, the linearity of the PID controllers is convenient because of the availability of basic physical parts (e.g. dampers, springs, RLC circuits, op-amps, etc...) that are capable of realizing these linear dynamics. However, this realization quickly becomes challenging when designing biomolecular controllers. This difficulty arises because (a) biomolecular controllers have to respect the structure of BioChemical Reaction Networks (BCRN), and (b) the quantities to be controlled (protein copy numbers or concentrations) cannot be negative (see [23] for positive integral control). Furthermore, the dynamics of biochemical reactions are inherently nonlinear. To achieve RPA, BCRN realizations of standalone Integral (I) controllers initially received the widest attention [24–29]. In previous work [26], the Antithetic Integral (aI) feedback controller was introduced to realize integral action that ensures RPA. In fact, more recently, it was shown in [10] that the antithetic motif is necessary to achieve RPA in arbitrary intracellular networks with noisy dynamics. A detailed mathematical analysis of the performance tradeoffs that may arise in the aI controller is presented in [30, 31], and optimal tuning is treated in [32]. Furthermore, practical design aspects, particularly the dilution effect of controller species, are addressed in [28, 29]. Biological implementations of various biomolecular integral controllers appeared in bacteria *in vivo* [7, 9, 10] and *in vitro* [14], and more recently in mammalian cells [15].

In the pursuit of designing high performance controllers while maintaining the RPA property, BCRN realizations of PI and PID controllers started receiving more focused attention [33–38]. Particularly in [33], a proportional component is separately appended to the antithetic integral motif via a repressing hill-type function to tune the transient dynamics and reduce the variance. The resulting PI controller follows the concept of Figure 1(d) where error and output feedback are used to build separate (but nonlinear) P and I components. Several successful attempts were carried out to devise BCRN realizations that approximate derivatives [39–43]. However, the first focused work on BCRN realizations of a full PID controller was reported in [35], where the authors introduced additional controller

species to obtain a derivative component. The resulting PID controller uses error feedback (similar to the concept of Figure 1(c)) to build separate nonlinear P, I, and D components and successfully improves the dynamic performance in the deterministic setting. Using a different approach, [37] and [38] exploit the dual-rail representation from [24], where additional species are introduced to overcome the non-negativity challenge of the realized PID controller. The authors demonstrate the resulting improvement of the performance in the deterministic setting. On a different note, [36] analyzed the effects of separate proportional and derivative controllers on (bursty) gene expression models in the stochastic setting.

Interestingly, all previous research in this direction have two intimately related aspects in common. Firstly, the P, I, and D components are realized separately such that they enter the dynamics additively. This aspect is motivated by traditional PID controllers where the controller dynamics are constrained to be linear, and thus the three components has to be added up (rather than multiplied for ex-

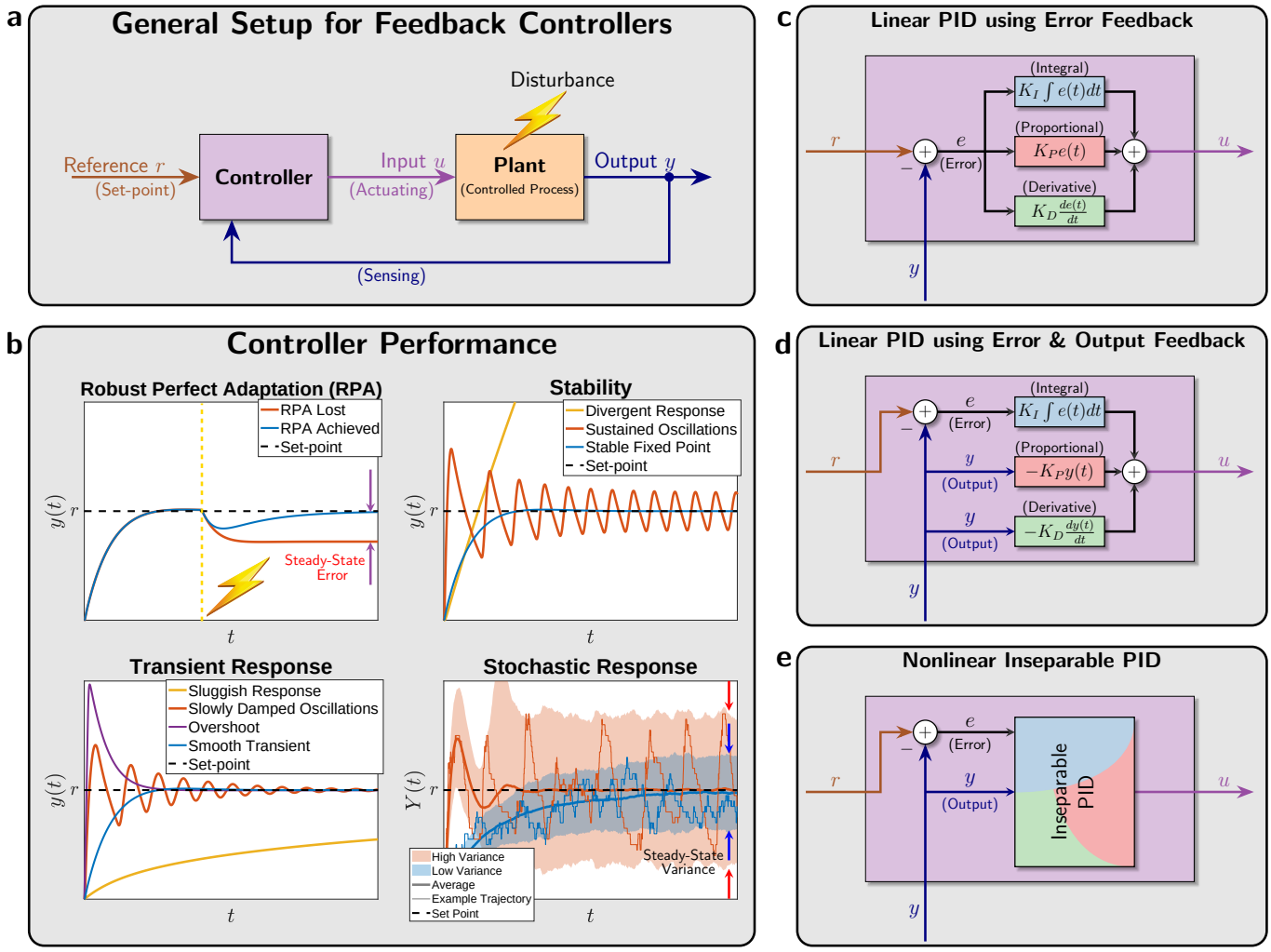

Figure 1: **Feedback controller design and performance. (a)** The output to be controlled is fed back into the controller via a sensing mechanism. The controller exploits the set-point, that is typically "dialed in" by the user and computes the suitable control action to be applied to the plant (or process) via an actuation mechanism. The goal of the control action is to steer the output to the desired set-point despite external or even internal disturbances. **(b)** A demonstration of four performance goals that are typically targeted when designing the controller. **Robust Perfect Adaptation (RPA)**: This is the biological analogue of the notion of *Robust Steady-State Tracking* (RSST) that is well known in control theory [1]. A controller achieves RPA if it drives the steady state of the plant output y to the set-point (or reference, denoted by r) despite varying initial conditions, plant uncertainties and/or constant disturbances. **Stability Enhancement**: A typical goal of a controller is to stabilize the dynamics. That is, it forces the output y to converge to a fixed steady-state value thus avoiding divergent responses and sustained oscillations. **Desirable Transient Response**: Another typical control objective is to yield a smooth transient response which is fast enough but doesn't overshoot or oscillate too much. **Variance Reduction**: For stochastic dynamics, it is common to study the time evolution of the output probability distribution and its moments such as the mean and variance. A natural performance objective is to design a controller that tightens the probability distribution around the mean, e.g. reduce the variance (cell-to-cell variability). **(c), (d), and (e) Various PID control architectures.** The classical designs in (c) and (d) involve separate linear P, I and D operations that are added together to yield the control action u. The difference between (c) and (d) is in the controller input: in (c) the error signal is the only input, while in (d) the error signal is fed into the I component whereas the output signal is fed into the P and D components . In this paper, we propose PID control architectures that fit in the more general class depicted in (e) where the PID components may be nonlinear and inseparable. This gives more mathematical realization flexibility for biomolecular controllers.

ample). However, since feedback mechanisms in BCRNs are inherently nonlinear, there is no reason to restrict the controller to have linear dynamics and/or additive components. Secondly, the proposed designs introduce additional species to mathematically realize the controller, and thus making the biological implementation more difficult. To this end, we consider in this paper (more general) nonlinear PID controllers that do not have to be explicitly separable into their three (P, I and D) components. This allows controllers to involve P, I , and D architectures in one (inseparable) block as depicted in Figure 1(e) where both, error and output, feedbacks are allowed. The nonlinearity and inseparability features of the proposed PI and PID controllers provide more flexibility in the BCRN design and allows simpler architectures that do not require introducing additional species to the standalone integral controller. Next, we adopt a hierarchical approach to slightly increase the complexity of the controller designs by introducing up to two additional controller species. This approach offers the designer a natural compromise between simplicity and performance.

Results

General framework for biomolecular feedback controllers. The framework for feedback control systems is traditionally described through block diagrams (e.g. Figure 1(a)). In this section, we lay down a general framework for feedback control systems where both the plant and the controller are represented by Biochemical Reaction Networks (BCRN). With this framework, the controller can either represent an actual biomolecular circuit or it can be implemented as a mathematical algorithm *in silico* [44–46] to regulate a biological circuit (through light for example [47]).

Consider a general plant, depicted in Figure 2, comprised of L species $\mathbf{X} := \{\mathbf{X_1}, \cdots, \mathbf{X_L}\}$ that react with each other through K reaction channels labeled as $\mathcal{R} := \{\mathcal{R}^1, \mathcal{R}^2, \cdots, \mathcal{R}^K\}$. Each reaction $\mathcal{R}^k$ ($k = 1, 2, \cdots, K$) has a stoichiometry vector denoted by $\zeta_k \in \mathbb{Z}^L$ and a propensity function $\lambda_k : \mathbb{R}_+^L \to \mathbb{R}_+$. Let $S := \begin{bmatrix}\zeta_1 & \zeta_2 & \cdots & \zeta_K\end{bmatrix} \in \mathbb{Z}^{L\times K}$ denote the stoichiometry matrix and let $\lambda := \begin{bmatrix}\lambda_1 & \lambda_2 & \cdots & \lambda_K\end{bmatrix}^T$ denote the (vector-valued) propensity function. Then, the plant constitutes a BCRN that is fully characterized by the triplet $\mathcal{N} := (\mathbf{X}, S, \lambda)$ which we shall call the "open-loop" system.

The goal of this work is to design a controller network, denoted by $\mathcal{N}_c$, that is connected in feedback with the plant network $\mathcal{N}$, as illustrated in Figure 2(a), to meet certain performance objectives such as those mentioned in Figure 1(b). We assume that all the plant species are inaccessible by the controller except for species $\mathbf{X_1}$ and $\mathbf{X_L}$. Particularly, the controller "senses" the plant output species $\mathbf{X_L}$, then "processes" the sensed signal via the controller species $\mathbf{Z} := \{\mathbf{Z_1}, \cdots, \mathbf{Z_M}\}$, and "actuates" the plant input species $\mathbf{X_1}$. The controller species are allowed to react with each other and with the plant input/output species through K_c reaction channels labeled

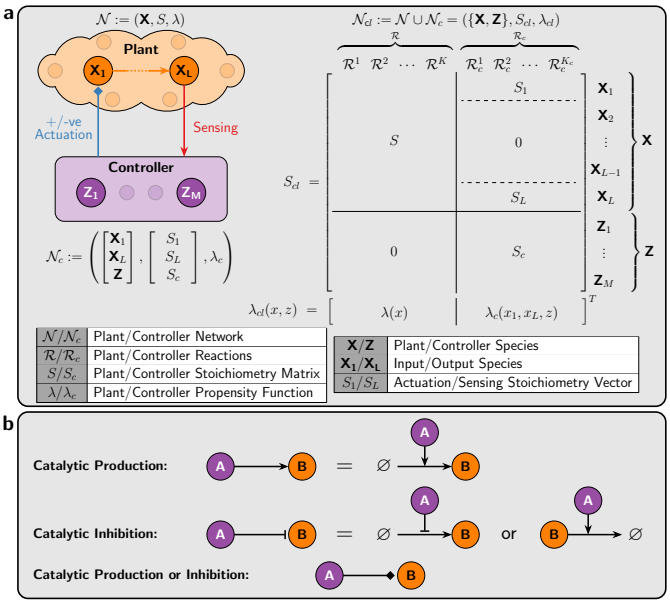

Figure 2: **A framework for feedback control of Chemical Reaction Networks. (a)** An arbitrary plant is comprised of L species $\{\mathbf{X_1}, \cdots, \mathbf{X_L}\}$ reacting with each other. Species $\mathbf{X_L}$, by definition, is the output of interest to be controlled, while $\mathbf{X_1}$ is assumed to be the only accessible input species that can be "actuated" (positively and/or negatively) by the controller network which is comprised of M species $\{\mathbf{Z_1}, \cdots, \mathbf{Z_M}\}$. The closed-loop system, with stiochiometry matrix S_{cl} and propensity function λ_{cl}, denotes the overall feedback interconnection between the plant and controller networks. The partitioning of S_{cl} and λ_{cl} describes the various components of the closed-loop network. **(b)** A description of the compact graphical notation that is adopted throughout the paper. Arrows directed toward species indicate catalytic productions, whereas T-shaped lines indicate catalytic inhibitions that encompass either repressive production or degradation. Note that the propensities of degradation reactions are considered to be either $kAB/(B+\kappa)$ if two parameters (k, κ) are indicated on the arrow, or ηAB if only one parameter η is indicated on the arrow. Finally, diamonds indicate either production or inhibition.

as $\mathcal{R}_c := \{\mathcal{R}_c^1, \mathcal{R}_c^2, \cdots, \mathcal{R}_c^{K_c}\}$. Let $\bar{S}_c \in \mathbb{Z}^{(M+2)\times K_c}$ and $\lambda_c : \mathbb{R}_+^{M+2} \to \mathbb{R}_+^{K_c}$ denote the stoichiometry matrix and propensity function of the controller, respectively. Since the controller reactions $\mathcal{R}_c$ involve the controller species $\mathbf{Z}$ and the plant input/output species $\mathbf{X_1}/\mathbf{X_L}$, the stoichiometry matrix $\bar{S}_c$ can be partitioned as

$$\bar{S}_c := \begin{bmatrix} S_1 \\ S_L \\ S_c \end{bmatrix},$$

where S_1 and $S_L \in \mathbb{Z}^{1\times K_c}$ encrypt the stoichiometry coefficients of the plant input and output species $\mathbf{X_1}$ and $\mathbf{X_L}$, respectively, among the controller reaction channels $\mathcal{R}_c$. Furthermore, $S_c \in \mathbb{Z}^{M\times K_c}$ encrypts the stoichiometry coefficients of the controller species $\mathbf{Z_1}$, $\cdots$, $\mathbf{Z_M}$. Hence, the controller design problem boils down to designing S_1, S_L, S_c and λ_c. Note that, for simplicity, we consider plants with Single-Input-Single-Output (SISO) Species. However, this can be straightforwardly generalized to Multiple-Input-Multiple-Output (MIMO) Species by adding more rows to S_1 and S_L. Finally, the closed-loop system constitutes the open-loop network ap-

pended by the controller network so that it includes all the plant and controller species $\mathbf{X_{cl}} := \{\mathbf{X}, \mathbf{Z}\}$ and reactions $\mathcal{R}_{cl} := \{\mathcal{R}, \mathcal{R}_c\}$. Thus, the closed-loop network, $\mathcal{N}_{cl} := \mathcal{N} \cup \mathcal{N}_c$, can be fully represented by the closed-loop stoichiometry matrix S_{cl} and propensity function λ_{cl} described in Figure 2(a). We close this section, by noting that our proposed controllers range from simple designs involving $M = 2$ controller species, up to more complex designs involving $M = 4$ controller species.

Antithetic Proportional-Integral (aPI) feedback controllers. Equipped with the BCRN framework for feedback control systems, we are now ready to propose several PI feedback controllers that are capable of achieving various performance objectives. All of the proposed controllers involve the antithetic integral motif introduced in [26] to ensure RPA. However, other additional motifs are appended to mathematically realize a Proportional (P) control action.

Consider the closed-loop network, depicted in Figure 3, where an arbitrary plant is connected in feedback with a class of controllers that we shall call aPI controllers. Observe that there are three different inhibition actions that are color coded. Each inhibition action gives rise to a single class of the proposed aPI controllers. Particularly, when no inhibition is present, we obtain the standalone antithetic Integral (aI) controller of [26] whose reactions are summarized in the left table of Figure 3. Whereas, aPI of Class 1 (resp. Class 2) involves the inhibition of $\mathbf{X_1}$ by $\mathbf{X_L}$ (resp. $\mathbf{Z_2}$), and aPI of Class 3 involves the inhibition of $\mathbf{Z_1}$ by $\mathbf{X_L}$. Furthermore, each aPI class encompasses various types of controllers depending on the inhibition mechanisms that enter the controller network as actuation reactions. We consider three types of biologically-relevant inhibition mechanisms detailed in Figure 3: additive, multiplicative (competitive) and degradation. Considering all three aPI classes with the various inhibition mechanisms, Figure 3 proposes eight different aPI control architectures. Note that, it can be shown that a degradation inhibition in the case of aPI Class 3 would destroy the RPA property and is thus omitted. All of these controllers are compactly represented by a single general closed-loop stoichiometry matrix S_{cl} and propensity function λ_{cl} depicted in Figure 3. The various architectures can be easily obtained by suitably selecting the functions $h := h^+ - h^-$ and g from the tables of Figure 3. A theoretical linear perturbation analysis is carried out in Section S1.1 of the SI to verify the proportional-integral control structure of the proposed controllers. In fact, the analysis applies to any smooth function h which is monotonically increasing (resp. decreasing) in z_1 (resp. z_2, x_1 and x_L), and any smooth function g which is monotonically increasing (resp. decreasing) in μ (resp. x_L).

Deterministic steady-state analysis: Robust Perfect Adaptation (RPA) of aPI controllers. The deterministic dynamics of the closed loop systems, for all the aPI controllers given in Figure 3 can be compactly written as a set of *Ordinary Differential Equations* (ODEs) given

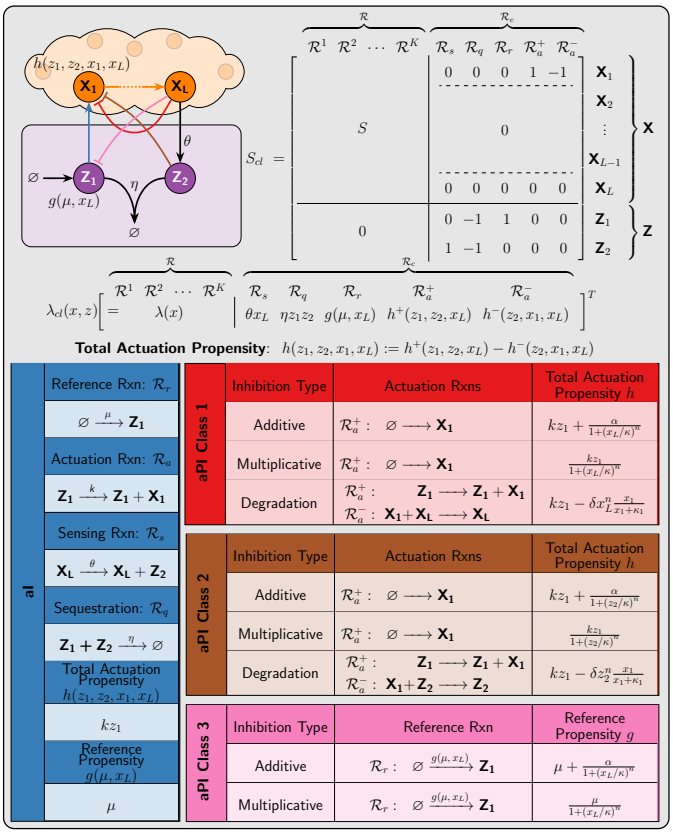

Figure 3: **Antithetic Proportional-Integral (aPI) feedback controllers.** Three different classes of aPI controllers are designed by appending the standalone aI controller with three inhibitions. Three biologically-relevant inhibition mechanisms are considered. **Additive Inhibition**: The inhibitor species produces the inhibited species separately at a decreasing rate. For instance, in the case of aPI Class 1 with additive inhibition, both $\mathbf{Z_1}$ and $\mathbf{X_L}$ produce $\mathbf{X_1}$ separately, but $\mathbf{Z_1}$ acts as an activator while $\mathbf{X_L}$ acts as a repressor. This separate inhibition can be modeled as the production of $\mathbf{X_1}$ as a positive actuation reaction $\mathcal{R}_a^+$ with an *additive* hill-type propensity given by $h^+(z_1, x_L) = kz_1 + \frac{\alpha}{1+(x_L/\kappa)^n}$, where n, α and κ denote the hill coefficient, maximal production rate and repression coefficient, respectively. This aPI is the closest control architecture to [33] and [35], since the P and I components are additive and separable (see Figures 1(c) and (d)). **Multiplicative Inhibition**: The inhibitor *competes* with an activator over a production reaction. In the case of aPI Class 1 with multiplicative inhibition, $\mathbf{X_L}$ inhibits the production of $\mathbf{X_1}$ by $\mathbf{Z_1}$. This can be modeled as the production of $\mathbf{X_1}$ with a *multiplicative* hill-type propensity given by $h^+(z_1, x_L) = kz_1 \times \frac{1}{1+(x_L/\kappa)^n}$. Observe that in this scenario, the Proportional (P) and Integral (I) control actions are inseparable; instead, this actuation reaction $\mathcal{R}_a^+$ encodes both PI actions simultaneously. **Degradation Inhibition:** The inhibitor invokes a negative actuation reaction that degrades the inhibited species. For instance, in the case of aPI Class 1 with degradation inhibition, $\mathbf{Z_1}$ produces $\mathbf{X_1}$ (positive actuation reaction $\mathcal{R}_a^+$), while $\mathbf{X_L}$ degrades $\mathbf{X_1}$ (negative actuation reaction $\mathcal{R}_a^-$). For generality, if the degradation is assumed to be n-cooperative, the dynamics can be captured by using a positive actuation with propensity $h^+(z_1) = kz_1$ and a negative actuation with propensity $h^-(x_1, x_L) = \delta x_1 x_L^n$. The total actuation propensity is defined as $h(z_1, x_1, x_L) := h^+(z_1) - h^-(x_1, x_L)$. The three classes with different inhibition mechanisms give rise to eight controllers that are compactly represented by the closed-loop stoichiometry matrix S_{cl} and propensity function λ_{cl} by choosing the suitable h functions from the tables.

by

$$\begin{cases} \dot{x} = S\lambda(x) + h(z_1, z_2, x_1, x_L)e_1 \\ \dot{z}_1 = g(\mu, x_L) - \eta z_1 z_2 \\ \dot{z}_2 = \theta x_L - \eta z_1 z_2, \end{cases} \tag{2}$$

where $e_1 := \begin{bmatrix} 1 & 0 & \cdots & 0 \end{bmatrix}^T \in \mathbb{Z}^L$. Note that the total actuation and reference propensities h and g take different forms for different aPI control architectures as depicted in Figure 3. The fixed point of the closed-loop dynamics cannot be calculated explicitly for a general plant; however, the output component (x_L) of the fixed point solves the following algebraic equation

$$g(\mu, \bar{x}_L) = \theta \bar{x}_L, \tag{3}$$

where over-bars denote steady-state values (if they exist), that is $\bar{x}_L := \lim_{t\to\infty} x_L(t)$. Two observations can be made based on (3). The first observation is that (3) has a unique nonnegative solution since g is a monotonically decreasing function in x_L. The second observation is that (3) does not depend on the plant. As a result, if the closed-loop system is stable (i.e. the dynamics converge to a fixed point), then the output concentration converges to a unique set-point that is independent of the plant. This property is valid for any initial condition, and is referred to as *Robust Perfect Adaptation* (RPA). Particularly, for the aI and aPI controllers of Class 1 and 2, the reference propensity is $g(\mu, x_L) = \mu$, and thus $\bar{x}_L = \frac{\mu}{\theta}$. Furthermore, for the aPI of Class 3, $\bar{x}_L$ solves a polynomial equation of degree $n+1$ (see Section S3 in the SI). In conclusion, all the proposed aPI controllers maintain the RPA property that is obtained by the antithetic integral motif, while introducing additional control knobs as extra degrees of freedom to enhance other performance objectives.

Deterministic stability analysis & performance assessment of aPI controllers. To compare the stability properties of the various proposed aPI controllers, we consider a particular plant, depicted in Figure 4(a), that is comprised of two species $\mathbf{X_1}$ and $\mathbf{X_2}$ ($L = 2$). This plant may represent a gene expression network where $\mathbf{X_1}$ is the mRNA that is translated to a protein $\mathbf{X_2}$ at a rate k_1. The degradation rates of $\mathbf{X_1}$ and $\mathbf{X_2}$ are denoted by γ_1 and γ_2, respectively. The closed-loop stoichiometry matrix and propensity function are also shown in Figure 4(a). Using the Routh-Hurwitz stability criterion, one can establish the exact conditions of local stability of the fixed point (Equation (S17) in Section S3 of the SI) for the various proposed aPI controllers. These conditions, once satisfied, guarantee that the dynamics locally converge to the fixed point.

For the remainder of this section, we consider fast sequestration reactions, that is, η is large. Under this assumption, one can obtain simpler stability conditions that are calculated in Section S3 of the SI, and tabulated in Figure 4(b). The stability conditions are given as inequalities that has to be satisfied by the various parameters of the closed-loop systems. A particularly significant lumped parameter group is $\rho := \frac{k k_1 \theta}{\gamma_1 \gamma_2 (\gamma_1 + \gamma_2)}$ that depends only on the plant and standalone aI controller parameters. To study the stabilizing effect of the appended proportional (P) component, we fix all the parameters related to the plant and standalone aI controller (hence ρ is fixed), and investigate the effect of the other controller parameters related to the appended proportional component. By examining the table in Figure 4(b), one can see that, compared to the standalone aI, the aPI controller of Class 1 with multiplicative (resp. degradation) inhibition enhances stability regardless of the exact values of κ (resp. δ) and n. This gives rise to a structural stability property: adding these types of proportional components guarantees better stability without having to fine-tune parameters.

In contrast, although the aPI controller of Class 1 with additive inhibition may enhance stability, special care has to be taken when tuning α. In fact, if α is tuned to be larger than a threshold given by $\alpha_{TH} := \frac{\gamma_1 \gamma_2}{k_1} r \left[1 + (r/\kappa)^n\right]$, then stability is lost. Figure 4(c) elaborates more on this type of aPI controller. Three cases arise here. Firstly, if $\rho < 1$, that is the standalone aI already stabilizes the closed-loop dynamics, then the (α, κ)-parameter space is split into a stable and unstable region. In the latter ($\alpha > \alpha_{TH}$), z_2 grows to infinity, and the output x_2 never reaches the desired set-point $r = \mu/\theta$. Secondly, if $1 < \rho < 2$, that is the standalone aI is unstable, then the (α, κ)-parameter space is split into three regions: (1) a stable region, (2) an unstable region with divergent response similar to the previous scenario where $\rho < 1$, and (3) another unstable region where sustained oscillations emerge as depicted in the bottom plot of Figure 4(c). Note that the closer ρ is to 2, the narrower the stable region is. Thirdly, for $\rho > 2$, the stable region disappears and thus this aPI controller has no hope of stabilizing the dynamics without re-tuning the parameters related to the standalone aI controller (e.g. k and/or θ). Clearly, multiplicative and degradation inhibitions outperform additive inhibition if stability is a critical objective. To this end, Figure 4(d) shows how the settling time and overshoot can be tuned by the controller parameters α, κ, and δ for additive, multiplicative, and degradation inhibitions, respectively. It is shown that with multiplicative and degradation inhibitions, one can simultaneously suppress oscillations (settling time) and remove overshoots. In contrast, a proportional component with additive inhibition can suppress oscillations but is not capable of removing overshoots as illustrated in the simulations of Figure 4(d) to the right. Furthermore, one can lose stability if α is increased above a threshold as mentioned earlier. Nevertheless, for multiplicative and degradation inhibitions, increasing the controller parameters (κ^{-1}, δ) too much can make the response slower but can never destroy stability.

It can be shown that the other two classes (2 and 3) are undesirable in enhancing stability. For instance, observe that for Class 2, the stability conditions are the same as the standalone aI controller (in the limit as $\eta \to \infty$) with an exception in the case of additive inhibition when

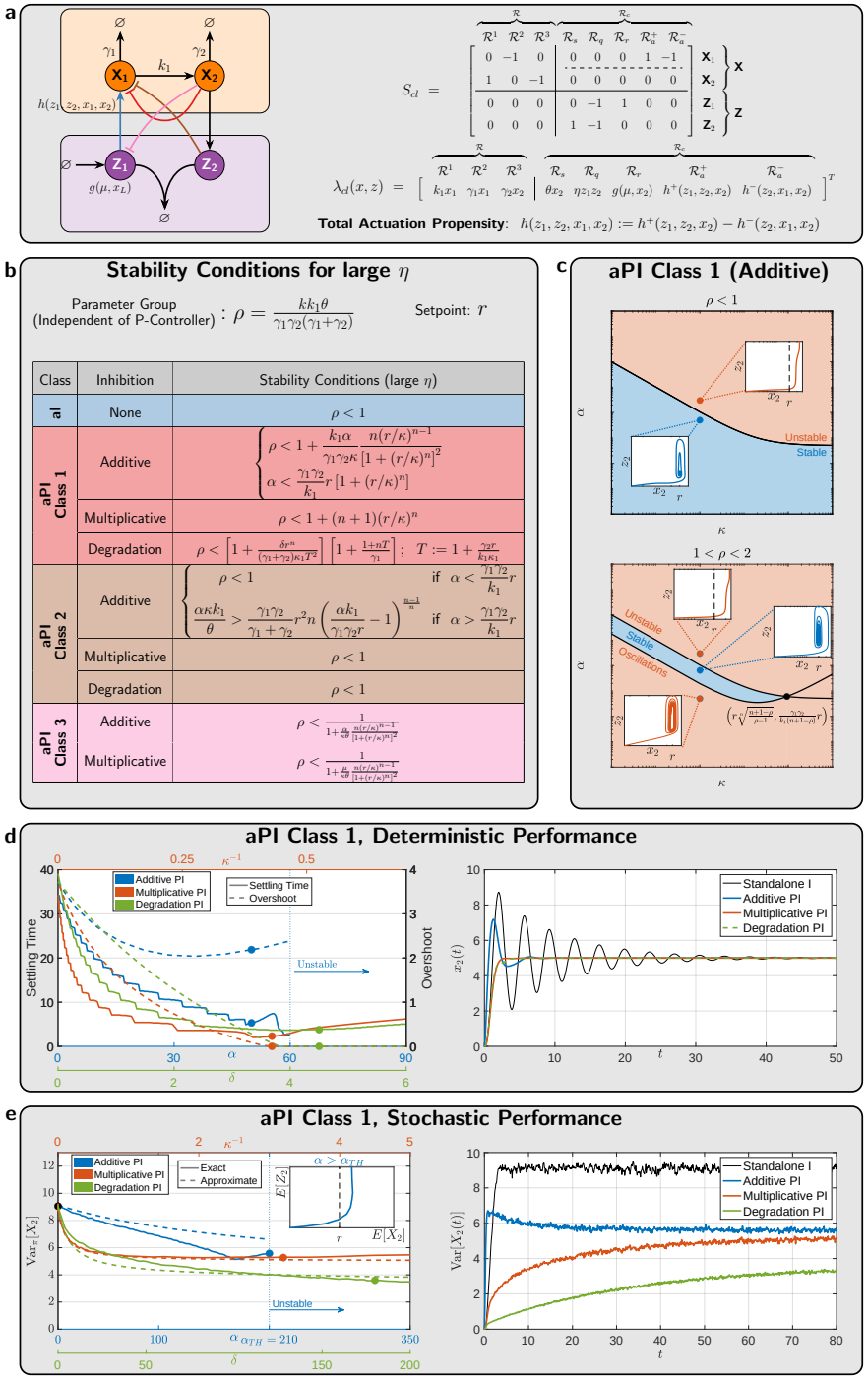

Figure 4: **Performance of aPI feedback controllers. (a)** Gene expression network controlled by aPI controllers. **(b)** Inequalities that need to be respected by the various controllers (with η is large enough) to guarantee closed-loop stability in the deterministic setting. Multiplicative and degradation inhibition mechanisms exhibit superior structural stability properties. **(c)** aPI controllers of class 1 with an additive inhibition mechanism, exhibit different stability properties for different ranges of the parameter group ρ (that depends solely on the plant and the standalone aI controller). In particular, for $\rho < 2$, the additive proportional control action can stabilize the dynamics, while for $\rho > 2$, it cannot stabilize without re-tuning the integral component. **(d)** Settling time and overshoot for the output ($\mathbf{X_2}$) response as a function of controller parameters that are related to the appended proportional components. Multiplicative and degradation inhibition mechanisms are capable of ameliorating the performance without risking instability as opposed to the additive inhibition mechanism. **(e)** Reduction of the output stationary variance with aPI controllers. The aPI controllers of Class 1 with all three inhibition mechanisms are capable of reducing the stationary variance of the output. This is demonstrated here via the simulations and the approximate formula shown in Table 1 as well. For additive inhibition, α has a threshold value α_{TH} above which ergodicity is lost similar to deterministic setting. Furthermore, observe that for values of α that are close to α_{TH}, the analytic approximation is less accurate. In contrast, the multiplicative and degradation mechanisms are capable of reducing the variance without the risk of losing ergodicity, and the analytic approximation remains accurate. The numerical values of all the parameters can be found in Section S8 in the SI.

$\alpha > \frac{\gamma_1\gamma_2}{k_1} r$. In this case, the inequality is structurally very different from all other stability conditions. In fact, the actuation via $\mathbf{Z_2}$ dominates $\mathbf{Z_1}$, and hence $\mathbf{Z_2}$ becomes responsible for the Integral (I) action instead of $\mathbf{Z_1}$. The detailed analysis of this network is not within the scope of this paper, and is left for future work. Finally, aPI controllers of Class 3 deteriorates the stability margin, since the right hand side of the inequalities are strictly less than one. However, this class of controllers can be useful for slow plants if the objective is to speed up the dynamics.

Stochastic analysis of the aPI controllers: RPA & stationary variance. We now investigate the effect of the aPI controllers on the stationary (steady-state) behavior of the output species $\mathbf{X_L}$ in the stochastic setting. Particularly, we examine the stationary expectation $\mathbb{E}_\pi[X_L]$ and variance $\text{Var}_\pi[X_L]$. The evolution of the expectations of the various species in the closed-loop network of Figure 3 are simply given by the differential equation $\frac{d}{dt}\mathbb{E}[X_{cl}] = \mathbb{E}[S_{cl}\lambda_{cl}(X_{cl})]$. By substituting for the closed-loop stoichiometry matrix S_{cl} and propensity function λ_{cl} given in Figure 3, we obtain the following set of differential equations that describe the evolution of the expectations for

Stationary Variance $\mathrm{Var}_\pi[X_2] \approx r\left[\frac{(\gamma_1+\gamma_2+\sigma_3)(\gamma_1\gamma_2+\gamma_2\sigma_3+\sigma_1 k_1)+k_1\gamma_2(\gamma_1+\sigma_4)}{(\gamma_1+\gamma_2+\sigma_3)(\gamma_1\gamma_2+\gamma_2\sigma_3+k_1\sigma_4)-\sigma_1 k_1\theta}\right]$					
Controller	$h^+(z_1,x_2)$	$h^-(x_1,x_2)$	$\sigma_1 = K_I$	σ_3	$\sigma_4 = K_{P_1}$
aI	kz_1	0	k	0	0
aPI Class 1 (Additive Inhibition)	$kz_1 + \frac{\alpha}{1+(x_2/\kappa)^n}$	0	k	0	$\frac{\alpha}{r}\frac{n(r/\kappa)^n}{[1+(r/\kappa)^n]^2}$
aPI Class 1 (Multiplicative Inhibition)	$\frac{kz_1}{1+(x_2/\kappa)^n}$	0	$\frac{k}{1+(r/\kappa)^n}$	0	$\frac{\gamma_1\gamma_2}{k_1}\frac{n(r/\kappa)^n}{1+(r/\kappa)^n}$
aPI Class 1 (Degradation Inhibition)	kz_1	$\delta x_2^n \frac{x_1}{x_1+\kappa_1}$	k	$\delta r^n \frac{\kappa_1}{\left(\frac{\gamma_2}{k_1}r+\kappa_1\right)^2}$	$nr^n\frac{\delta\gamma_2/k_1}{\frac{\gamma_2}{k_1}r+\kappa_1}$

Table 1: An approximate analytic formula for the output stationary variance of a gene expression network regulated by the aPI controllers of Class 1 with various inhibition mechanisms. Recall that the total actuation propensity is defined as $h := h^+ - h^-$, and its Jacobian is defined by $\partial h(\bar{z}_1,\bar{x}_1,\bar{x}_2) =: \begin{bmatrix}\sigma_1 & -\sigma_3 & -\sigma_4\end{bmatrix}$ with $\sigma_1 > 0$ and $\sigma_3,\sigma_4 \geq 0$. Furthermore, recall from Equation (S2) in the SI that the proportional gain $K_{P_1} = \sigma_4$ and the integral gain $K_I = \frac{\sigma_1\bar{z}_1+\sigma_2\bar{z}_2}{\bar{z}_1+\bar{z}_2}$. Since in the limit of large η, $\bar{z}_2 \approx 0$ (refer to Section S7 in the SI), then $K_I \approx \sigma_1$. Observe that the denominator of the variance expression is positive if the deterministic setting is stable (see Equation (S18) in the SI). Hence this expression is only valid when the deterministic setting is stable; otherwise, this approximation is meaningless. For additive inhibition (which is similar to the previous works in [33] and [35] with $\kappa = n = 1$), α tunes the proportional gain separately. In fact, increasing α decreases the stationary variance as demonstrated in Figure 4(e) through both stochastic simulations and the approximate analytic formula. In contrast, for the case of multiplicative inhibition, tuning κ automatically tunes both the proportional and integral gains in a beneficial manner to the stationary variance. More precisely, decreasing κ increases the proportional gain $K_{P_1} = \sigma_4$ and decreases the integral gain $K_I \approx \sigma_1$, simultaneously. This has the effect of decreasing the variance without risking loss of stability as demonstrated in Figure 4(e). Finally, for degradation inhibition, increasing δ also increases the proportional gain and thus reduces the stationary variance as well.

an arbitraty plant.

$$\begin{cases} \frac{d}{dt}\mathbb{E}[X] = \mathbb{E}[S\lambda(X)] + \mathbb{E}[h(z_1,z_2,x_1,x_L)] \\ \frac{d}{dt}\mathbb{E}[Z_1] = \mathbb{E}[g(\mu,X_L)] - \eta\mathbb{E}[Z_1Z_2] \\ \frac{d}{dt}\mathbb{E}[Z_2] = \theta\mathbb{E}[X_L] - \eta\mathbb{E}[Z_1Z_2]\,. \end{cases} \tag{4}$$

At stationarity, assuming that the closed-loop network is ergodic, the time derivatives are set to zero. Particularly, we have

$$\frac{d}{dt}\left(\mathbb{E}_\pi[Z_1] - \mathbb{E}_\pi[Z_2]\right) = 0 \implies \mathbb{E}_\pi[g(\mu,X_L)] = \theta\mathbb{E}_\pi[X_L]\,.$$

To achieve RPA at the population level (i.e. expectations), the stationary expectation $\mathbb{E}_\pi[X_L]$ of the output species should not depend on the plant parameters. Clearly, this depends on the function g. In fact, if g is nonlinear in X_L, then there is no guarantee that RPA is achieved because the nonlinearity couples higher order moments (that may depend on the plant parameters) with $\mathbb{E}_\pi[X_L]$. As a result, RPA is not guaranteed for the aPI controllers of Class 3 in the stochastic setting, although it is guaranteed in the deterministic setting. Nonetheless if g is affine in X_L, then RPA is guaranteed (once again, assuming ergodicity). In particular, for the aPI controllers of Class 1 and 2, we have $g(\mu,X_L) = \mu$ and as a result $\mathbb{E}_\pi[X_L] = \mu/\theta =: r$. Clearly, for these classes of controllers, $\mathbb{E}_\pi[X_L]$ depends only on the control parameters μ and θ (like the deterministic setting), and thus RPA is ensured as long as the closed-loop network is ergodic.

Next, we examine the variance of the output species $\mathbf{X_L}$. Unfortunately, a general analysis for an arbitrary plant cannot be done. As a case study, we consider again the particular plant given in Figure 4(a) in feedback with the aPI controller of Class 1. Note that the subsequent analysis can be generalized to any (affine-linear) plant with mono-molecular reactions. Even for this particular plant, one cannot derive an exact expression for $\mathrm{Var}_\pi[X_2]$. This is a consequence of the moment closure problem that stems from the inherent nonlinear nature of the antithetic motif (quadratic propensity: $\eta z_1 z_2$) and the proportional control (propensity: $h(z_1,z_2,x_1,x_2)$). However, a tailored moment closure technique was proposed in [33] to give an approximate expression for $\mathrm{Var}_\pi[X_2]$ in the case of the aPI controller of Class 1 with additive inhibition and $n = \kappa = 1$. This approximate technique exploits the fact that $\mathbb{E}_\pi[Z_1Z_2] = \mu/\eta \approx 0$ for large η; and as a result assumes that Z_2 remains close to zero. Furthermore, a linearized approximation of the function h is also exploited to circumvent the moment closure problem. Extending this approximate technique to our more general controllers allows us to give a general (approximate) expression for $\mathrm{Var}_\pi[X_2]$ that encompasses all three types of inhibitions with an arbitrary hill coefficient $n \geq 1$. The results are summarized in Table 1, where a general formula is given for any choice of h. One can easily see from the general expression in Table 1 that $\mathrm{Var}_\pi[X_2]$ is monotonically increasing in the integral gain $K_I \approx \sigma_1$ and monotonically decreasing in the proportional gain $K_{P_1} = \sigma_4$. This conclusion extends the results in [33] to more general proportional actuations involving different mechanisms of inhibitions and with cooperativity ($n \geq 1$). Figure 4(e) demonstrates this stationary variance reduction via simulations and the approximate formula given in Table 1. Unlike additive inhibition, multiplicative and degradation inhibitions provide a structural property of decreasing the stationary variance of the output species $\mathbf{X_2}$ without risking the loss of ergodicity (similar to the deterministic setting).

Antithetic Proportional-Integral-Derivative feedback (aPID) controllers. In this section, we append a Derivative (D) control action to the aPI (Class 1) controller of Figure 3 to obtain an array of aPID controllers depicted in Figure 5. The proposed aPID controllers range from simple second order (involving only two controller species $\mathbf{Z_1}$ and $\mathbf{Z_2}$) up to fourth order (involving four controller species $\mathbf{Z_1}$ to $\mathbf{Z_4}$). Furthermore the various controllers are categorized as two types: N-Type and P-Type. N-Type (Negative feedback) controllers are usually suitable for plants with positive gain (increasing the input yields an increase in the output), while P-Type (Positive feedback) controllers are usually suitable for plants with negative gains. This ensures that the overall control loops realize negative feedback. Note that one can easily construct hybrid PN-Type controllers, where the individual P, I and D components have different P/N-Types. This hybrid design is shown to be very useful for certain plants (see Figure 7(d) for example).

We start with the N-Type second order design (first row of Figure 5) whose main advantage is its simplicity. Intuitively, the antithetic integral motif is cascaded with an Incoherent FeedForward Loop (IFFL) to yield a PID architecture whose P, I and D components are inseparable as described in Figure 1(e). More precisely, the output species $\mathbf{X_L}$ directly inhibits $\mathbf{X_1}$ and simultaneously produces it via the intermediate species $\mathbf{Z_1}$. As a result, $\mathbf{Z_1}$ simultaneously plays the role of both an intermediate species for the IFFL and the AIF control action. It is shown in Section S1.2.1 in the SI that this simple design embeds a (low-pass) filtered PID controller. The N-Type third order design (second row of Figure 5) involves one additional controller species $\mathbf{Z_3}$ to realize an IFFL that is disjoint from the antithetic motif. This yields an inseparable PD component appended to the separate I controller. It is shown in Section S1.2.2 in the SI that this design embeds a (low-pass) filtered PD + I controller when η is large enough. In contrast, the N-Type fourth order design (third row of Figure 5) involves two additional controller species $\mathbf{Z_3}$ and $\mathbf{Z_4}$ to realize a completely separable PID control architecture. It is shown in Sections S1.2.3 and S1.2.4 in the SI that this design embeds a PI + (low-pass) filtered D controller when η and η_0 are large enough. The key idea behind mathematically realizing the derivative component here is fundamentally different from the previous two designs. This controller realizes an "antithetic differentiator", where the antithetic motif feeds back into itself: $\mathbf{Z_3}$ feeds back into $\mathbf{Z_4}$ via the rate function $g(z_3, x_L)$. In fact, this idea is inspired by a well-known concept in control theory (see Section S6 in the SI) which basically exploits an integral controller, in feedback with itself to implement a low-pass filtered derivative controller. For this fourth order design, the derivative action can be achieved in two ways. One way is by mutually producing $\mathbf{Z_4}$ and $\mathbf{X_1}$ at a rate $g(z_3, x_L)$ such that g is monotonically increasing (resp. decreasing) in z_3 (resp. x_L). This implementation is treated separately in Section S1.2.3 of the SI. The other way is by producing $\mathbf{Z_4}$ while degrading $\mathbf{X_1}$ at a mutual rate of $g(z_3, x_L)$ such that g is monotonically increasing in both z_3 and x_L. This implementation is treated separately in Section S1.2.4 of the SI. Both designs have the same underlying PID control structure, but one might be easier to experimentally implement than the other.

It is straightforward to show that the set-point for the second order design is given by $\bar{x}_L = \frac{\mu}{\theta-\beta}$ with the requirement that $\beta < \theta$; whereas the set-point for both higher order designs are given by $\bar{x}_L = \frac{\mu}{\theta}$. Furthermore, the effective PID gains, denoted by (K_P, K_I, K_D), and cutoff frequency ω of the embedded low-pass filter for each of the proposed aPID controllers can be designed by tuning the various biomolecular parameters: $\beta, \eta, \eta_0, \gamma_0, \mu_0$ and the parameters of the propensity functions h and g. These functions, serving as an implementation choice, can be picked in a similar fashion to the aPI controllers in the tables of Figure 3 depending on the inhibition mechanism to be implemented (additive, multiplicative or degradation). In the subsequent examples, we use degradation inhibitions, but the other mechanisms can also be used.

Next, we demonstrate various properties of the proposed controller designs in the deterministic setting. The mappings between the effective PID parameters (K_P, K_I, K_D, ω) and the biomolecular parameters $(\mu, \theta, \eta, \beta, \gamma_0, \eta_0, ...)$ are given in S4 of the SI for each controller. It is fairly straightforward to go back and forth between the two parameter spaces. For control analysis, these mappings can compute the various PID parameters from the biomolecular parameters; whereas, for control design, these mappings can compute the various biomolecular parameters that achieve some desired PID gains and cutoff frequency. As a result, one can use existing methods in the literature (eg. [48]) to carry out the controller tuning in the PID parameter space, and then map them to the actual biomolecular parameter space. Nevertheless, it is of critical importance to note that different controllers yield different coverage over the PID parameter space. For instance, for the fourth order design, there are enough biomolecular degrees of freedom to design any desired positive $(K_P, K_I, K_D, \omega) \in \mathbb{R}^4_+$. The lower the order of the controller, the less the biomolecular degrees of freedom, and hence the more constrained the coverage in the PID parameter space. For instance, for the third order design, the achievable PID parameters are constrained to satisfy $K_P \leq K_D\omega$. For the second order design, the constraint becomes even stricter. The details are all rigorously reported in Section S4 of the SI.

We first show the limitation of aPI controllers, and then demonstrate the flexibility that comes with an added derivative component. We also show that the higher order controllers exhibit more flexibility in shaping the transient response. Consider the controlled gene expression network depicted in Figure 6(a) where the ordinary differential equations of the various controllers are shown to explicitly specify the adopted propensity functions h and g. In this example, we consider both the P and D components acting on the input species $\mathbf{X_1}$ as negative actuation via degradation reactions. We start by highlighting the fun-

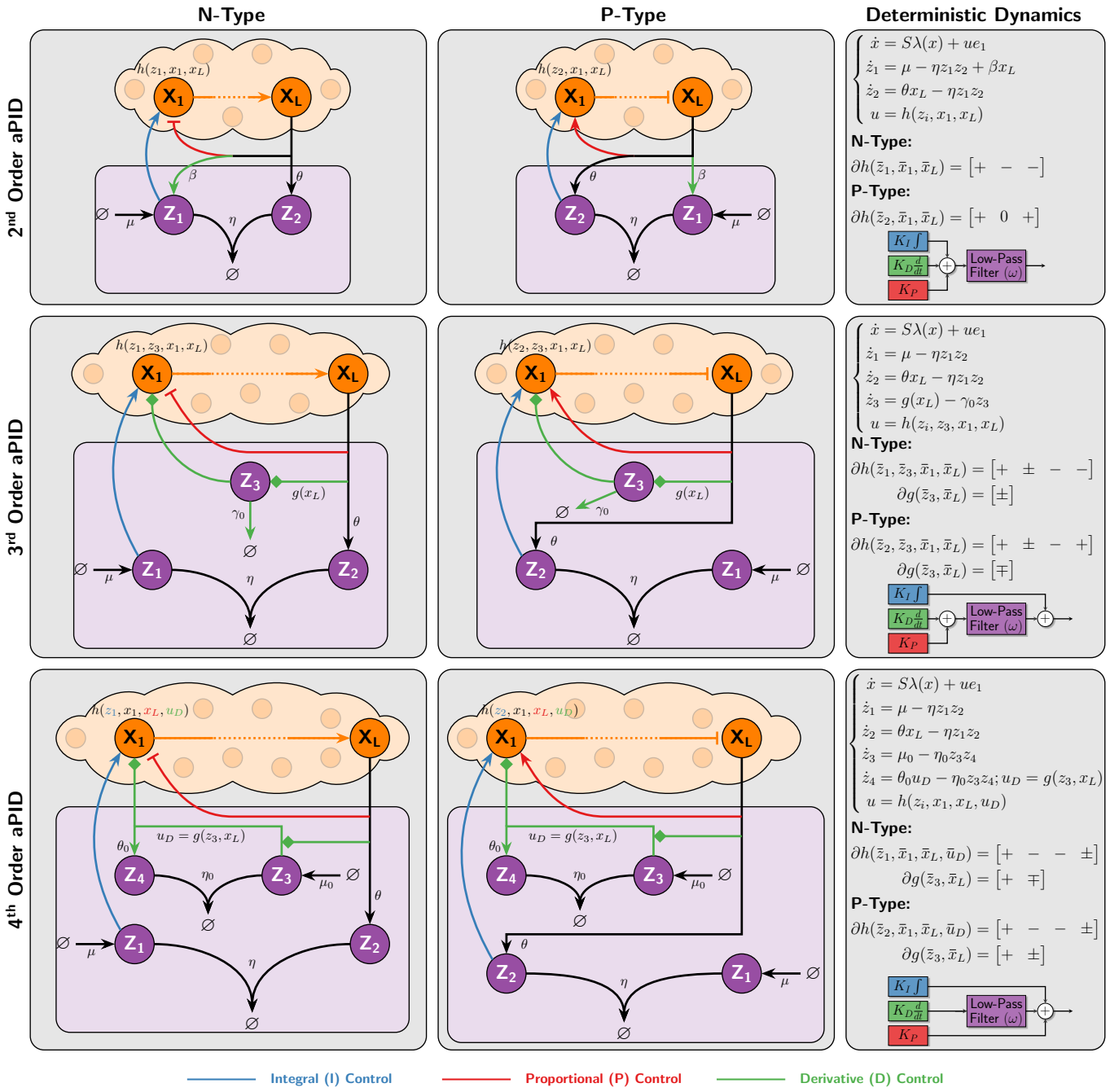

Figure 5: **Antithetic Proportional-Integral-Derivative (aPID) feedback controllers.** N-Type (Negative feedback) controllers are usually suitable for plants with positive gain (increasing the input yields an increase in the output), while P-Type (Positive feedback) controllers are usually suitable for plants with negative gains. The order of the controllers indicate the number of controller species $\mathbf{Z_i}$. The second order aPID controller has the simplest design where no additional species are added to the aPI design, and only one reaction is added to produce $\mathbf{Z_1}$ catalytically from $\mathbf{X_L}$ at a rate $\beta < \theta$. The third order aPID controller adds a single species to the aPI design. This intermediate species $\mathbf{Z_3}$ is produced by the output $\mathbf{X_L}$ and actuates the input species $\mathbf{X_1}$. These actions (indicated by the diamonds) are allowed to be either activations or both inhibitions. Finally, the fourth order aPID controller adds two species to the aPI design. These two species form an antithetic differentiator where $\mathbf{Z_3}$ is constitutively produced at a rate μ_0 and participates with $\mathbf{Z_4}$ in a sequestration reaction with a rate η_0. For the N-Type design, the derivative action enters the plant either by mutually producing $\mathbf{Z_4}$ and $\mathbf{X_1}$ at a rate $g(z_3, x_L)$ (see Figure S4) such that g is monotonically increasing (resp. decreasing) in z_3 (resp. x_L), or by producing $\mathbf{Z_4}$ while degrading $\mathbf{X_1}$ at a mutual rate of $g(z_3, x_L)$ (see Figure S5) such that g is monotonically increasing in both z_3 and x_L. Intuitively, the second and third order aPID controllers mathematically realize a derivative action using an incoherent feedforward loop from $\mathbf{X_L}$ to $\mathbf{X_1}$ via $\mathbf{Z_1}$ and $\mathbf{Z_3}$, respectively; whereas the fourth order aPID controller realizes a derivative action by placing an additional antithetic integral motif in feedback with the plant and itself ($\mathbf{Z_3}$ feeds back into $\mathbf{Z_4}$).

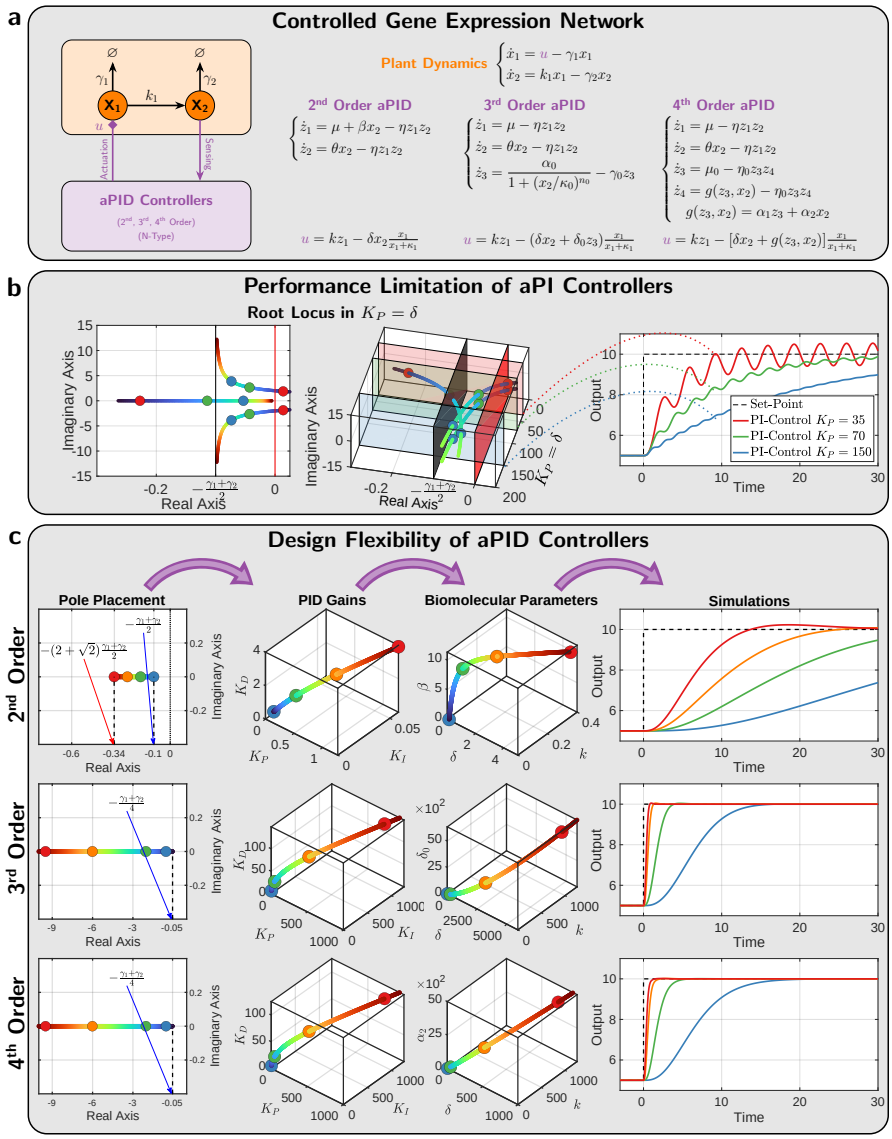

Figure 6: ***a*PID control of a gene expression network . (a) Closed-loop dynamics.** A gene expression network is controlled by the various N-Type aPID controllers of Figure 5. The deterministic dynamics and the overall control action u are shown here for each controller to explicitly specify the adopted propensity functions h and g in this example. **(b) Fundamental limitation of *a*PI controllers.** The left and middle plots demonstrate the same root locus of the linearized dynamics as K_P is increased. The left plot depicts the complex plane, while the middle plot explicitly shows the complex plane together with the values of the proportional gain K_P which is shown to be approximately equal to δ. These plots verify that two eigenvalues are confined within a small region close to the imaginary axis when γ_1 and γ_2 are small, and thus imposing a limitation on the achievable performance as demonstrated in the simulations shown in the right plot. **(c) Design flexibility offered by derivative control actions.** Exploiting all the components of the full aPID controllers offer more flexibility in achieving superior performance compared to the aPI controllers. This panel shows the steps of a pole-placement, control design problem where the four dominant poles are placed on the real axis of the left-half plane to ensure a stable and non-oscillating response with a minimal overshoot. The second order aPID exhibits a restriction on how far to the left the poles can be placed; whereas the higher order controllers can place the poles arbitrarily as far to the left as desired and thus achieving a response that is as fast as desired without overshoots nor oscillations. The design problem starts by picking the poles, then computing the PID gains(shown here) and cutoff frequency (not shown here), and finally computing the actual biomolecular parameters that allows us to obtain the nonlinear simulations to the right.

damental limitation of aPID controllers alone (without a D) in Figure 6(b). Using simple root locus arguments (see Section S5.1), it is shown that two complex eigenvalues – of the linearized dynamics around the fixed point – approach a vertical asymptote at $-\frac{\gamma_1+\gamma_2}{2}$ as K_P is increased, while one real eigenvalue approaches the origin (due to integral control). This is numerically demonstrated in the two root-locus plots of Figure 6(a), where $K_P \approx \delta$ (for a sufficiently small κ_1). Clearly, the asymptotic limit is independent of all other parameters, including the integral gain K_I. This analysis highlights a fundamental limitation of the aPI controller, because no matter how we tune K_P and K_I, two of the eigenvalues are constrained to remain close to the imaginary axis when γ_1 and γ_2 are small. In the time domain, this is interpreted as being restricted to either a slowly rising response or a faster rising response but with slowly damped oscillations as illustrated in the simulation examples of Figure 6(b). This limitation can be mitigated by appending a derivative control action via the various aPID controllers. To demonstrate this, we consider a design problem where the end goal is to achieve a fast response without oscillations and with minimal overshoot. This can be achieved by placing the eigenvalues far to the left on the real axis. Hence the design problem boils down to the following objective: place the four most dominant eigenvalues (or poles) at $s = -a$ where $a > 0$ and make a as large as possible. The design steps start by first (1) deciding where to place the poles $s = -a$ for some desired a, then (2) computing the PID parameters – using equations (S46) in the SI – that place the poles as desired, and finally (3) mapping the PID parameters to the actual biomolecular parameters using the formulas in Section S4. This is pictorially demonstrated in Figure 6(c) for each aPID controller. However, it is shown in Section S5.2 of the SI that the second order aPID imposes a lower bound on the achievable poles given by $-(2+\sqrt{2})\frac{\gamma_1+\gamma_2}{2}$ as demonstrated in Figure 6(c). As a result, with a second order aPID, the performance can be made better than the aPI controller; however, the performance is also limited and cannot be made faster than a threshold – dictated by γ_1 and γ_2 – without causing overshoots and/or oscillations. In contrast, it is also shown in Section S5.2 of the SI that

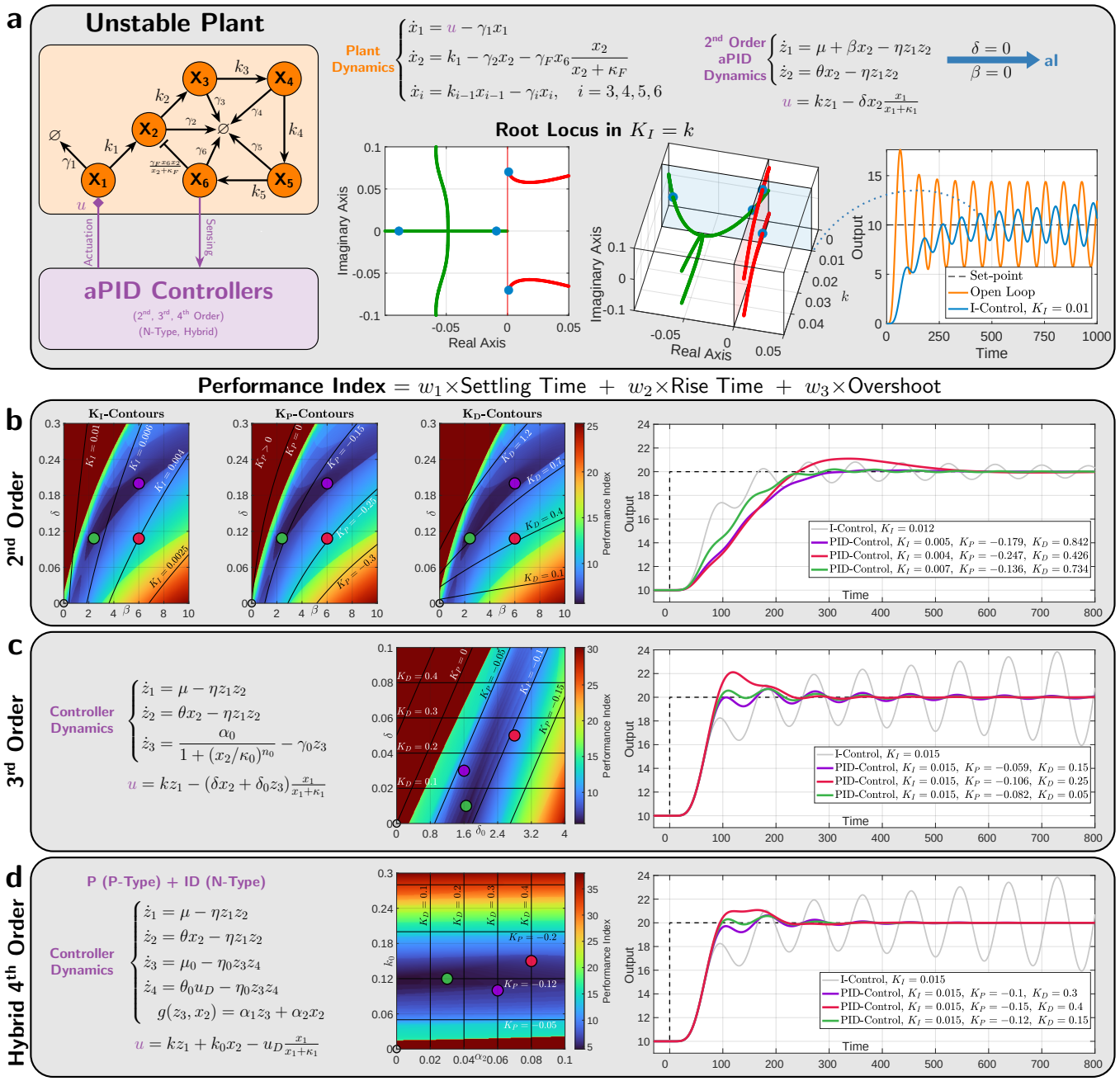

Figure 7: ***a*PID control of an unstable and more complex plant. (a) Plant description.** The plant considered here involves $L = 6$ species and embeds a negative feedback from $\mathbf{X_6}$ to $\mathbf{X_2}$ via an active degradation reaction. The underlying deterministic dynamics of the plant and the second order *a*PID controller are shown in this panel. It is demonstrated that the open loop is unstable (orange response), and integral control alone cannot stabilize the dynamics since two eigenvalues carry on a positive real part for any $k \geq 0$. **(b), (c) and (d) Performance of the various *a*PID controllers.** The intensity plots show the Performance Index over a range of biomolecular parameter values. These plots are overlaid with contours where the PID gains K_P, K_I or K_D are constant. For the third and fourth order *a*PID in **(c)** and **(d)**, $K_I \approx k$ and thus can be tuned separately with k which is held constant throughout this figure. For the fourth order *a*PID in **(d)**, the K_P- and K_D-contours are orthogonal to the k_0- and α_2-axes, respectively, and hence can also be tuned separately. For the third order *a*PID in **(c)**, the K_D-contours are orthogonal to the δ-axis and hence K_P can be tuned separately with δ_0; whereas, the inseparability of the PD components forces the K_P-contours to be oblique and thus δ tunes both K_P and K_D simultaneously. Finally, for the second order *a*PID in **(b)**, all three contours are not orthogonal to the axes and, as a result, all three PID gains have to be mutually tuned by the biomolecular parameters. This is due to the inseparability of all PID components. Note that each set of contours are displayed on a separate intensity plot here for clarity. Observe that the optimal performance for each controller is located in the dark blue regions where the proportional gains K_P are negative. Three different examples, red, green and purple (along with the unstable standalone *a*I control in blue), are picked to demonstrate the achievable high performances depicted in the response plots to the right. For the second and third order *a*PID, negative K_P can be achieved by properly tuning the biomolecular parameters without having to switch the topology from N-Type to P-Type. However, for the (separable) fourth order *a*PID controller, a hybrid design with N-Type ID and P-Type P can also achieve a negative K_P which is critical for controlling this plant.

the third and fourth order aPID can make a as big as desired without any theoretical upper bound. This means that the added complexity of the higher order controllers are capable of shaping the response of the gene expression network freely and as fast as desired with no overshoots nor oscillations. This is also demonstrated in the simulations depicted in Figure 6(c).

Next, we consider a more complex plant to be controlled. The plant, comprised of $L = 6$ species, is depicted in Figure 7(a) where $\mathbf{X_i}$ degrades at a rate γ_i and catalytically produces $\mathbf{X_{i+1}}$ at a rate k_i. Furthermore, the output species $\mathbf{X_6}$ feeds back into $\mathbf{X_2}$ by catalytically degrading it at a rate γ_F. This plant is adopted from [35]; however, to challenge our controllers more, the feedback degradation rate γ_F is chosen to be larger to yield a plant that is unstable when operating in open loop as shown in Figure 7(a). In fact, the root locus in the integral gain $K_I \approx k$ (for large η) demonstrates that this plant cannot be stabilized with a standalone aI controller, that is no matter how we tune k, the response will remain unstable. It is shown in [35] that, for this plant, the P control is not useful. This is the case because the proportional gain K_P was restricted to have a positive value. One of the nice features of our proposed second and third order aPID controllers is their ability to achieve negative proportional gains K_P (see (S27) and (S32) in the SI) without having to rewire, that is without switching topologically from N-Type to P-Type. This is a consequence of the inseparability of the P component from other components (I and D for the second order, and D for the third order). In Figures 7(b) and (c) we show that, for this plant, tuning K_P to be negative is critical to achieve a high performance where oscillations and overshoots are almost completely removed while maintaining a fast response. This is demonstrated using the intensity plots of a performance index that quantifies the overshoot, settling time and rise time of the output response over a range of the relevant biomolecular controller parameters. With the completely separable fourth order aPID, the gains cannot be tuned to be negative; however, one can always switch between N-Type and P-Type topologies or even resort to hybrid designs where different PID components are of different P/N Types. For instance, Figure 7(d) shows that by using a fourth order hybrid aPID controller, a high performance is achieved.

To demonstrate the effectiveness of aPID control of high dimensional plants, we consider the control of cholesterol levels in the plasma depicted in Figure 8. High levels of cholesterol, particularly Low-Density Lipoprotein-Cholesterol (LDL-C), serve as a major trigger for cardiovascular disease. To circumvent that, the body possesses natural pathways to regulate cholesterol homeostasis [50]. However, these regulatory mechanisms have the tendency to fail with age leading to elevated levels of plasma cholesterol due to metabolic disorders and/or poor nutrition [51]. A whole body mathematical model of cholesterol metabolism is adopted from [49] and is briefly described in Figure 8 (see [49] for details). The mathematical model of the cholesterol network is comprised of 34 state variables (species) and 43 parameters whose values are taken from https://www.ebi.ac.uk/biomodels/ where the model is coded in SBML format (MODEL 1206010000). Two different disturbances are applied: (1) an increase in daily dietary intake and (2) an increase in intestinal absorption. A second order aPID controller is connected in feedback with the network to regulate the LDL-C level and keep it at 100 mg/dL despite the disturbances. A positive actuation is realized by the production of the Intestinal Cholesterol (IC) via $\mathbf{Z_1}$ (blue arrow); whereas, a negative actuation is realized by the degradation of the IC via LDL-C (red T-shaped line). With positive integral actuation alone, the controller cannot achieve RPA because both disturbances increase the levels of LDL-C. Hence, without negative actuation the controller cannot restore the set-point. However, the aPID controller appends a negative

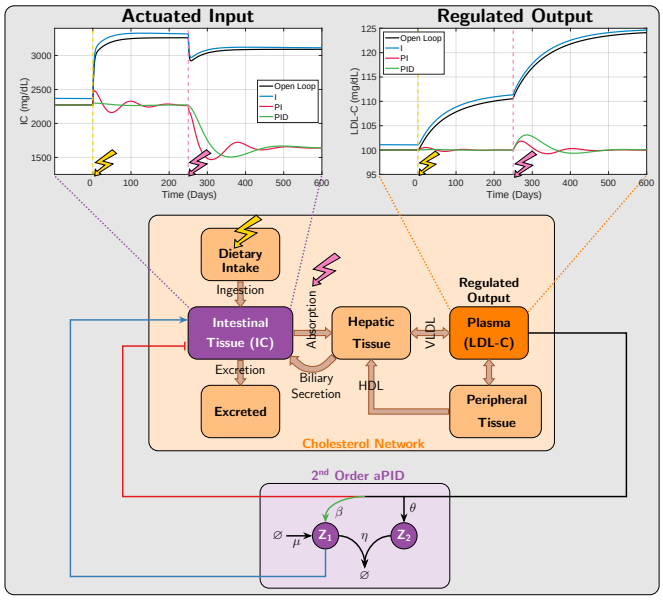

Figure 8: **aPID Control of a whole-body model of Cholesterol metabolism.** A whole-body model that describes the dynamics of cholesterol metabolism is adopted from [49]. The model tracks the flow of cholesterol, in its different forms, around the body. In summary, the Intestinal Cholesterol (IC) comes from the daily dietary intake or via biliary secretion from the liver (Hepatic Tissue). It is also locally synthesized in the intestine as well. The IC is either excreted from the body or absorbed and transported to the liver where it is then exported into the plasma via the Very-Low-Density Lipoproteins (VLDL). Excess cholesterol in the peripheral tissue is transferred to the liver via the High-Density Lipoproteins (HDL). Two exogenous disturbances are considered here: a 304 mg/day increase of dietary intake at $t_1 = 0$ and 25% increase in absorption at $t_2 = 250$ days. The first disturbance reflects a change in the daily diet, while the second reflects an increase of intestinal absorption efficiency. Both of these disturbances give rise to an increase in cholesterol levels in the plasma when no feedback control is applied as demonstrated in the black curve of right plot. To implement the simplest (second order) aPID control *in silico*, the IC is considered here to be the actuated input species, such that $\mathbf{Z_1}$ produces IC, while the output species $\mathbf{LDL-C}$ degrades IC. The response of both the input and regulated output are shown here to demonstrate that an I alone (with positive actuation) is incapable of achieving RPA; whereas adding a PD (with negative actuation), not only achieves RPA, but also reduces oscillations.

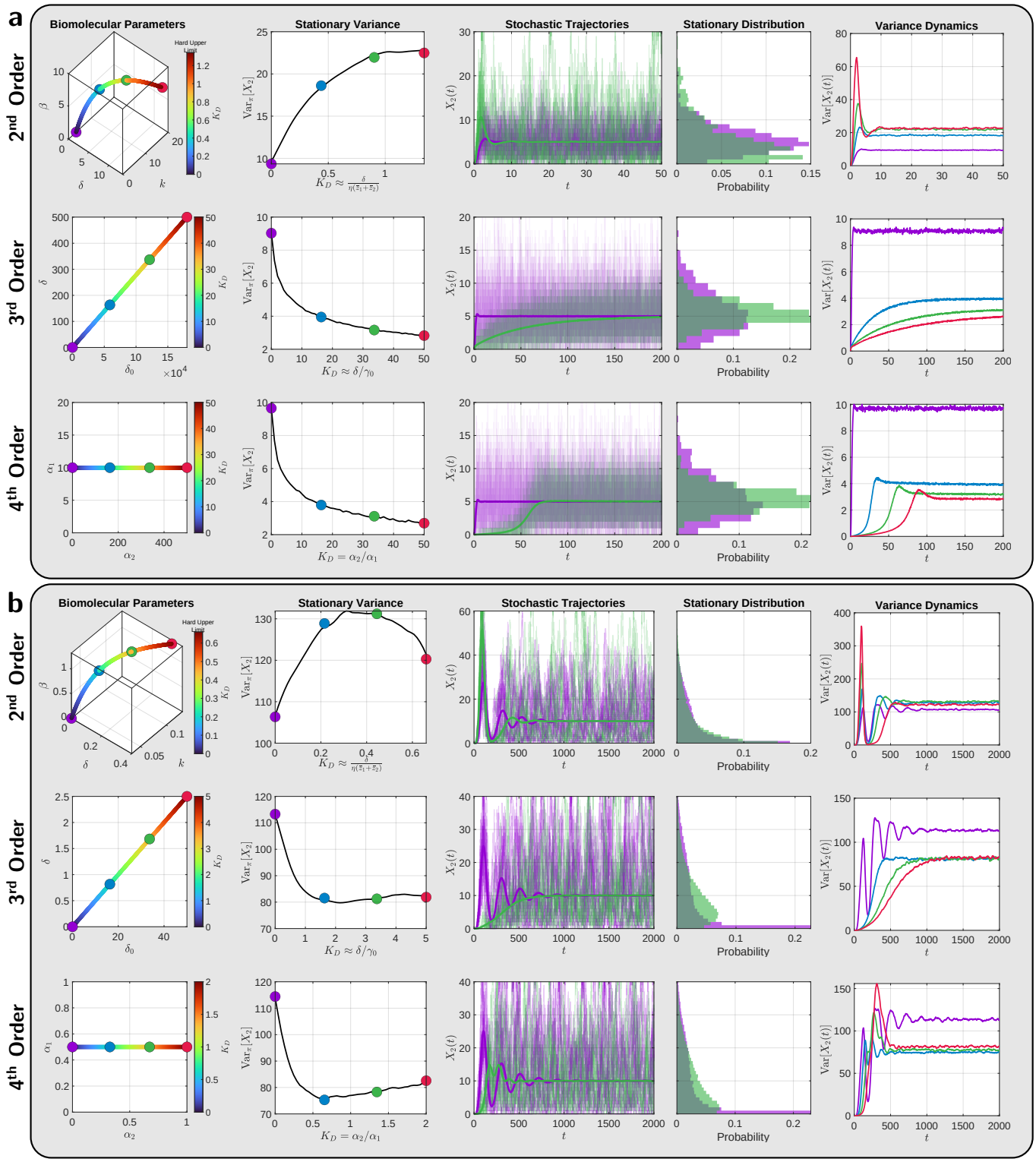

Figure 9: **Stochastic performance of the aPID feedback controllers.** In **(a)**, the plant is the gene expression network; whereas in **(b)**, the plant is the 6-Species network from Figure 7(a) but with stable open-loop dynamics (γ_F is chosen to be smaller). For both networks, the biomolecular parameters are chosen such that the integral gain K_I is constant and the proportional gain $K_P = 0$, while the derivative gain K_D is increased to track the effect of the derivative control action on the stationary variance of the output $\mathrm{Var}_\pi[X_2]$. The first column shows the selected biomolecular parameters that achieve the desired values of K_D, while the second column shows the stationary variance as a function of K_D. The third and fourth columns show the stochastic (single-cell) trajectories and stationary distribution of the output for two particular values of K_D (in green and purple). The fifth column shows the evolution of the variance in time for the four selected values of K_D. These simulations demonstrate that the derivative control action increases the stationary variance of the output for second order aPID design, while it is capable of reducing the variance considerably for the higher order aPID designs. In fact, for the gene expression plant, the variance can be reduced to a level lower than the mean value = 5.

actuation and is capable of achieving RPA of LDL-C levels and also of suppressing the overshoots and oscillations for both IC and LDL-C.

Effect of derivative control on the stationary variance. In this section, we examine the effect of the derivative component in the various aPID controllers on the cell-to-cell variability (e.g. stationary variance). We consider two plants: the gene expression network of Figure 6(a) and the six-species network of Figure 7(a). We fix the integral gain K_I to be a constant and set the proportional gain K_P to zero while we sweep the derivative gain K_D. The biomolecular parameters that achieve these gains can be easily calculated using the mappings in Section S4 in the SI. The simulation results are depicted in Figure 9. Unlike the higher order aPID controllers, the second order aPID exhibits a hard upper limit on the achievable values of K_D (see S27 in the SI). Figure 9 demonstrates that, for both plants, the third and fourth order aPID controllers are capable of reducing the stationary variance; whereas, the second order aPID increases it.

Alternative differentiators. In Figure 5, the antithetic integral motif is exploited to yield an antithetic differentiator; however, other integral motifs such as zero-order [53], [52] and auto-catalytic [25] integrators can also be similarly exploited as depicted in Figure S8 of the SI. These differentiators can be carefully appended to the aPI controllers of Class 1 (see Figure 3) to obtain an alternative set of aPID controllers depicted in Figure 10. Observe that these differentiators act on the concentration x_L of the output species to approximate its derivative as a rate $u_D := g(z_3, x_L)$. This is one of the differences between our differentiators and those proposed in [43] where the computed derivative is encoded as a concentration of another species. Having the computed derivative encoded directly as a rate rather than a concentration is particularly convenient for controllers with a fewer number of species. Another technical difference is that our differentiators realize a derivative with a first order low-pass filter; whereas, the differentiators in [43] realize derivatives with a second order low-pass filter due to the additional species introduced. We close this section by noting that it is also possible to replace the antithetic integral motif by other integrators to design yet another collection of PID controllers (see Figure S9 of the SI).

Discussion

This paper proposes a library of PID controllers that can be realized via biochemical reaction networks. The proposed PID designs are introduced as a hierarchy of controllers ranging from simple to more complex designs. This hierarchical approach that we adopt offers the designer a rich library of controllers that gives rise to a natural compromise between simplicity and achievable performance. At the lower end of the hierarchy, we introduce simple PID controllers that are mathematically realized with a small number of biomolecular species and reactions making them easier to implement biologically. As we move up in the hierarchy, more biomolecular species and/or reactions are introduced to push the limit on the achievable performance. More precisely, higher order PID controllers cover a wider range of PID gains that can be tuned to further enhance performance. Of course, this comes at the price of more complex designs making the controllers more difficult to implement biologically. The details of the biological implementations with specific parts are not within the scope of this paper but will be presented elsewhere.

In this work, we start by introducing a library of PI controllers based on the antithetic integral motif [26] and an appended feedback control action where the input species is directly actuated by the output species. This is similar in spirit to previous works in [33] and [35] where the proportional control action enters the dynamics additively via a separate repressive production reaction. While this mechanism succeeds in enhancing the overall performance, we introduce other biologically-relevant mechanisms, for the P component, that are capable of achieving even higher performance without risking instability and further reducing the stationary variance (see Figure 4). However, it is shown rigorously and through simulations (see Figure 6) that a PI controller alone is limited, while adding a D component adds more flexibility. Interestingly, it is shown that the performance of a gene expression network can be arbitrarily enhanced with full PID controllers: the PID can be tuned to achieve an arbitrarily fast response without triggering any oscillations or overshoots. This example highlights the power of full PID control. Another nice feature of PID control is the availability of various systematic tuning methods in the literature (see [48] for example). Well-known design tools in control theory (such as the pole placement performed in Figure 6) can be exploited to perform the tuning in the PID parameter space instead of the biomolecular parameter space. Then the obtained PID parameters (PID gains and cutoff frequency) can be mapped by the formulas we derived (see Section S4) to the actual biomolecular parameters. This novel approach considerably facilitates the biomolecular tuning process. It is worth mentioning that the biomolecular tuning is the easiest for the fourth order aPID due to the separability of its components which allows tuning each PID gain separately with a different biomolecular parameter. In contrast, the lower order aPID controllers mix the various P, I, and D components and render them inseparable (see Figure 1(e)) which results in each biomolecular parameter tuning multiple gains simultaneously. This is the price one has to pay for obtaining simpler designs. However, this can also be leveraged in some cases. For example, a single biomolecular parameter can tune both the integral and proportional gains simultaneously to enhance the dynamics and variance without risking instability (see the multiplicative aPI in Figure 4). This inseparability also offers a nice advantage where the proportional gains can be tuned to be negative without having to switch topologies from N-Type to P-Type. For certain plants, achieving negative gains is

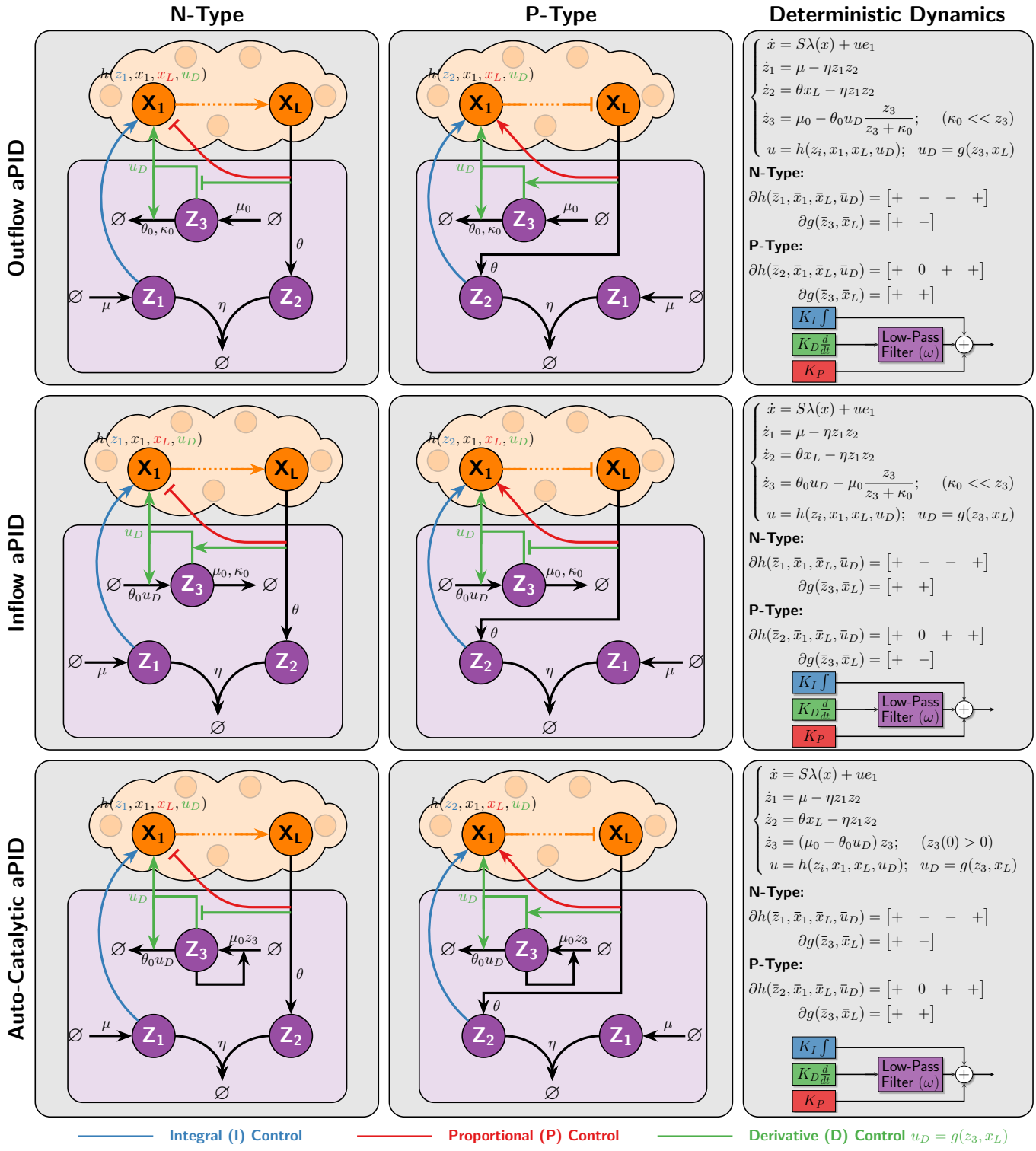

Figure 10: **PID controllers using integral-based differentiators.** Three differentiators are constructed based on three different integrators. The differentiators appended to the aPI controllers of Class 1 (see Figure 3) give rise to another collection of aPID controllers of both N- and P-Types. The Inflow and Outflow aPID controllers are based on integrators realized via zeroth-order degradation reactions [52], [53]. It is shown in Section S6 in the SI that if these degradation reactions are tuned to operate in a saturating regime ($\kappa_0 << z_3$), then a low-pass filtered derivative action is mathematically realized. The difference between the outflow and inflow aPID controllers is that the feedback action $u_D := g(z_3, x_L)$ which approximates the derivative of x_L enters through a degradation and production reaction of the additional controller species $\mathbf{Z_3}$, respectively. In contrast, the auto-catalytic aPID controller is based on an auto-catalytic integrator [25] where the additional control species $\mathbf{Z_3}$ produces itself. It is shown that for this component to properly function as a differentiator, the initial concentration of $\mathbf{Z_3}$ has to be non-zero and g has to be designed such that $g(0, x_L) = 0$ (see Section S6 in the SI).

critical to achieve a high performance (see Figure 7).

We would like to point out that the proposed control structures are all designed based on linear perturbation analysis (see Section S1 in the SI). This is motivated by the rich set of existing tools to design and analyze linear control systems; whereas nonlinear control design and analysis is challenging and is often treated on a case-by-case basis. In the linearization, the PID structures are verified and hence the dynamics behave exactly like what is expected from classical PID control. However, full nonlinear simulations are always carried out to back up the theoretical analyses and implications. Of course, the dynamical behavior of the nonlinear PID controllers may deviate from their linear counterparts when the dynamics are (initially) far from the fixed point. This is a limitation that we believe can serve as a good future research direction where small signal analysis should be extended to large signal analysis as well. Furthermore, in our work we lay down a general mathematical framework for biomolecular feedback control systems which can be used to pave the way for other possible controllers in the future. We believe that research along these directions helps building high performance controllers that are capable of reliably manipulating genetic circuits for various applications in synthetic biology and bio-medicine in the same way that PID controllers revolutionized other engineering disciplines such as navigation, telephony, aerospace, etc.

Acknowledgments

This project has received funding from the European Research Council (ERC) under the European Union's Horizon 2020 research and innovation programme (CyberGenetics; grant agreement 743269), and from the European Union's Horizon 2020 research and innovation programme (COSY-BIO; grant agreement 766840).

Competing Interests

ETH Zürich has filed a patent application on behalf of the inventors T.F., C.H.C., M.F. and M.K. that includes the designs described (application no. EP21187316.1).

References

[1] M. H. Khammash, "Robust steady-state tracking," *IEEE transactions on automatic control*, vol. 40, no. 11, pp. 1872–1880, 1995.

[2] T.-M. Yi, Y. Huang, M. I. Simon, and J. Doyle, "Robust perfect adaptation in bacterial chemotaxis through integral feedback control," *Proceedings of the National Academy of Sciences*, vol. 97, no. 9, pp. 4649–4653, 2000.

[3] D. Muzzey, C. A. Gómez-Uribe, J. T. Mettetal, and A. van Oudenaarden, "A systems-level analysis of perfect adaptation in yeast osmoregulation," *Cell*, vol. 138, no. 1, pp. 160–171, 2009.

[4] H. El-Samad, J. Goff, and M. Khammash, "Calcium homeostasis and parturient hypocalcemia: an integral feedback perspective," *Journal of theoretical biology*, vol. 214, no. 1, pp. 17–29, 2002.

[5] M. J. Dunlop, J. D. Keasling, and A. Mukhopadhyay, "A model for improving microbial biofuel production using a synthetic feedback loop," *Systems and synthetic biology*, vol. 4, no. 2, pp. 95–104, 2010.

[6] J. A. Stapleton, K. Endo, Y. Fujita, K. Hayashi, M. Takinoue, H. Saito, and T. Inoue, "Feedback control of protein expression in mammalian cells by tunable synthetic translational inhibition," *ACS synthetic biology*, vol. 1, no. 3, pp. 83–88, 2012.

[7] G. Lillacci, S. Aoki, D. Schweingruber, and M. Khammash, "A synthetic integral feedback controller for robust tunable regulation in bacteria," *BioRxiv*, p. 170951, 2017.

[8] A. H. Ng, T. H. Nguyen, M. Gomez-Schiavon, G. Dods, R. A. Langan, S. E. Boyken, J. A. Samson, L. M. Waldburger, J. E. Dueber, D. Baker, *et al.*, "Modular and tunable biological feedback control using a de novo protein switch," *Nature*, vol. 572, no. 7768, pp. 265–269, 2019.

[9] H.-H. Huang, Y. Qian, and D. Del Vecchio, "A quasi-integral controller for adaptation of genetic modules to variable ribosome demand," *Nature communications*, vol. 9, no. 1, pp. 1–12, 2018.

[10] S. K. Aoki, G. Lillacci, A. Gupta, A. Baumschlager, D. Schweingruber, and M. Khammash, "A universal biomolecular integral feedback controller for robust perfect adaptation," *Nature*, p. 1, 2019.

[11] G. Lillacci, Y. Benenson, and M. Khammash, "Synthetic control systems for high performance gene expression in mammalian cells," *Nucleic acids research*, vol. 46, no. 18, pp. 9855–9863, 2018.

[12] V. Hsiao, E. L. De Los Santos, W. R. Whitaker, J. E. Dueber, and R. M. Murray, "Design and implementation of a biomolecular concentration tracker," *ACS synthetic biology*, vol. 4, no. 2, pp. 150–161, 2015.

[13] C. L. Kelly, A. W. K. Harris, H. Steel, E. J. Hancock, J. T. Heap, and A. Papachristodoulou, "Synthetic negative feedback circuits using engineered small rnas," *Nucleic acids research*, vol. 46, no. 18, pp. 9875–9889, 2018.

[14] D. K. Agrawal, R. Marshall, V. Noireaux, and E. D. Sontag, "In vitro implementation of robust gene regulation in a synthetic biomolecular integral controller," *Nature communications*, vol. 10, no. 1, pp. 1–12, 2019.

[15] T. Frei, C.-H. Chang, M. Filo, and M. Khammash, "Genetically engineered integral feedback controllers for robust perfect adaptation in mammalian cells," *bioRxiv*, 2020.

[16] B. A. Francis and W. M. Wonham, "The internal model principle of control theory," *Automatica*, vol. 12, no. 5, pp. 457–465, 1976.

[17] N. Minorsky, "Directional stability of automatically steered bodies," *Journal of the American Society for Naval Engineers*, vol. 34, no. 2, pp. 280–309, 1922.

[18] R. Vilanova and A. Visioli, *PID control in the third millennium*. Springer, 2012.

[19] T. L. Blevins, "Pid advances in industrial control," *IFAC Proceedings Volumes*, vol. 45, no. 3, pp. 23–28, 2012.

[20] J. Li and Y. Li, "Dynamic analysis and pid control for a quadrotor," in *2011 IEEE International Conference on Mechatronics and Automation*, pp. 573–578, IEEE, 2011.

[21] S. Bennett, "A brief history of automatic control," *IEEE Control Systems Magazine*, vol. 16, no. 3, pp. 17–25, 1996.

[22] K. J. Åström and R. M. Murray, *Feedback systems: an introduction for scientists and engineers*. Princeton university press, 2010.

[23] C. Briat, "A biology-inspired approach to the positive integral control of positive systems: The antithetic, exponential, and logistic integral controllers," *SIAM Journal on Applied Dynamical Systems*, vol. 19, no. 1, pp. 619–664, 2020.

[24] K. Oishi and E. Klavins, "Biomolecular implementation of linear i/o systems," *IET systems biology*, vol. 5, no. 4, pp. 252–260, 2011.

[25] C. Briat, C. Zechner, and M. Khammash, "Design of a synthetic integral feedback circuit: dynamic analysis and dna implementation," *ACS Synthetic Biology*, vol. 5, no. 10, pp. 1108–1116, 2016.

[26] C. Briat, A. Gupta, and M. Khammash, "Antithetic integral feedback ensures robust perfect adaptation in noisy biomolecular networks," *Cell systems*, vol. 2, no. 1, pp. 15–26, 2016.

[27] F. Xiao and J. C. Doyle, "Robust perfect adaptation in biomolecular reaction networks," in *2018 IEEE Conference on Decision and Control (CDC)*, pp. 4345–4352, IEEE, 2018.

[28] Y. Qian and D. Del Vecchio, "Realizing 'integral control'in living cells: how to overcome leaky integration due to dilution?," *Journal of The Royal Society Interface*, vol. 15, no. 139, p. 20170902, 2018.

[29] C. C. Samaniego and E. Franco, "Ultrasensitive molecular controllers for quasi-integral feedback," *Cell Systems*, 2021.

[30] N. Olsman, F. Xiao, and J. C. Doyle, "Architectural principles for characterizing the performance of antithetic integral feedback networks," *Iscience*, vol. 14, pp. 277–291, 2019.

[31] N. Olsman, A.-A. Baetica, F. Xiao, Y. P. Leong, R. M. Murray, and J. C. Doyle, "Hard limits and performance tradeoffs in a class of antithetic integral feedback networks," *Cell systems*, vol. 9, no. 1, pp. 49–63, 2019.

[32] M. Filo and M. Khammash, "Optimal parameter tuning of feedback controllers with application to biomolecular antithetic integral control," in *2019 IEEE 58th Conference on Decision and Control (CDC)*, pp. 951–957, IEEE, 2019.

[33] C. Briat, A. Gupta, and M. Khammash, "Antithetic proportional-integral feedback for reduced variance and improved control performance of stochastic reaction networks," *Journal of The Royal Society Interface*, vol. 15, no. 143, p. 20180079, 2018.

[34] A. Gupta and M. Khammash, "An antithetic integral rein controller for bio-molecular networks," in *2019 IEEE 58th Conference on Decision and Control (CDC)*, pp. 2808–2813, IEEE, 2019.

[35] M. Chevalier, M. Gómez-Schiavon, A. H. Ng, and H. El-Samad, "Design and analysis of a proportional-integral-derivative controller with biological molecules," *Cell Systems*, vol. 9, no. 4, pp. 338–353, 2019.

[36] S. Modi, S. Dey, and A. Singh, "Proportional and derivative controllers for buffering noisy gene expression," in *2019 IEEE 58th Conference on Decision and Control (CDC)*, pp. 2832–2837, IEEE, 2019.

[37] N. M. Paulino, M. Foo, J. Kim, and D. G. Bates, "Pid and state feedback controllers using dna strand displacement reactions," *IEEE Control Systems Letters*, vol. 3, no. 4, pp. 805–810, 2019.

[38] M. Whitby, L. Cardelli, M. Kwiatkowska, L. Laurenti, M. Tribastone, and M. Tschaikowski, "Pid control of biochemical reaction networks," *IEEE Transactions on Automatic Control*, 2021.

[39] W. Halter, Z. A. Tuza, and F. Allgöwer, "Signal differentiation with genetic networks," *IFAC-PapersOnLine*, vol. 50, no. 1, pp. 10938–10943, 2017.

[40] W. Halter, R. M. Murray, and F. Allgöwer, "Analysis of primitive genetic interactions for the design of a genetic signal differentiator," *Synthetic Biology*, vol. 4, no. 1, p. ysz015, 2019.

[41] C. C. Samaniego, G. Giordano, and E. Franco, "Practical differentiation using ultrasensitive molecular circuits," in *2019 18th European Control Conference (ECC)*, pp. 692–697, IEEE, 2019.

[42] C. C. Samaniego, J. Kim, and E. Franco, "Sequestration and delays enable the synthesis of a molecular derivative operator," in *2020 59th IEEE Conference on Decision and Control (CDC)*, pp. 5106–5112, IEEE, 2020.

[43] E. Alexis, C. C. Schulte, L. Cardelli, and A. Papachristodoulou, "Biomolecular mechanisms for signal differentiation," *bioRxiv*, 2021.

[44] C. Guiver, H. Logemann, R. Rebarber, A. Bill, B. Tenhumberg, D. Hodgson, and S. Townley, "Integral control for population management," *Journal of Mathematical Biology*, vol. 70, no. 5, pp. 1015–1063, 2015.

[45] C. Briat and M. Khammash, "Computer control of gene expression: Robust setpoint tracking of protein mean and variance using integral feedback," in *2012 IEEE 51st IEEE Conference on Decision and Control (CDC)*, pp. 3582–3588, IEEE, 2012.

[46] C. Briat and M. Khammash, "Integral population control of a quadratic dimerization process," in *52nd IEEE Conference on Decision and Control*, pp. 3367–3372, IEEE, 2013.

[47] A. Milias-Argeitis, M. Rullan, S. K. Aoki, P. Buchmann, and M. Khammash, "Automated optogenetic feedback control for precise and robust regulation of gene expression and cell growth," *Nature communications*, vol. 7, no. 1, pp. 1–11, 2016.

[48] K. J. Åström and T. Hägglund, *PID controllers: theory, design, and tuning*, vol. 2. Instrument society of America Research Triangle Park, NC, 1995.

[49] M. T. Mc Auley, D. J. Wilkinson, J. J. Jones, and T. B. Kirkwood, "A whole-body mathematical model of cholesterol metabolism and its age-associated dysregulation," *BMC systems biology*, vol. 6, no. 1, pp. 1–21, 2012.

[50] J. Luo, H. Yang, and B.-L. Song, "Mechanisms and regulation of cholesterol homeostasis," *Nature reviews molecular cell biology*, vol. 21, no. 4, pp. 225–245, 2020.

[51] F. J. Félix-Redondo, M. Grau, and D. Fernández-Bergés, "Cholesterol and cardiovascular disease in the elderly. facts and gaps," *Aging and disease*, vol. 4, no. 3, p. 154, 2013.

[52] M. H. Khammash, "Perfect adaptation in biology," *Cell Systems*, vol. 12, no. 6, pp. 509–521, 2021.

[53] X. Y. Ni, T. Drengstig, and P. Ruoff, "The control of the controller: molecular mechanisms for robust perfect adaptation and temperature compensation," *Biophysical journal*, vol. 97, no. 5, pp. 1244–1253, 2009.